# UNIVERSITÀ DEGLI STUDI DI CAGLIARI

**PhD Programme**

**Molecular and Translational Medicine**

**Cycle XXXIII**

Department of Biomedical Sciences

Unit of Oncology and Molecular Pathology

# METABOLIC REPROGRAMMING IN ONCOGENE-DRIVEN HEPATOCELLULAR CARCINOMA: EFFECT OF LDHA KNOCK-DOWN

Scientific Disciplinary Code: Med/04


PhD student — Marina Serra

PhD Programme coordinator — Prof. Sebastiano Banni

Tutor — Prof. Amedeo Columbano


Final exam 2019 - 2020

Thesis defence: March 2021 Session

# ACKNOWLEDGEMENTS

Un ringraziamento sentito e profondo al Prof. Amedeo Columbano, il quale mi ha accolta nel suo gruppo di ricerca dandomi preziosi suggerimenti e continui incoraggiamenti, facendomi sentire da subito a casa. Devo a lui le motivazioni che mi hanno spinto a proseguire nel campo della ricerca, non facendomi mai mancare il suo sostegno anche nel periodo trascorso a Leuven. Grazie a tutto ciò mi sento una giovane ricercatrice pronta ad affrontare con positività ed entusiasmo le sfide che verranno.

Alla Prof.ssa Giovanna Maria Ledda la quale, pur avendo condiviso con me un periodo limitato del mio dottorato, mi ha sempre dato un importante supporto anche da lontano.

Al Prof. Andrea Perra un sincero ringraziamento per l'aiuto incessante e per i preziosi consigli che non sono mai venuti meno in questi tre anni.

Alla Dr.ssa Marta Anna Kowalik, per avermi trasmesso le sue conoscenze costituendo un importante appoggio nel mio percorso di dottorato.

Al Prof. Massimiliano Mazzone, per avermi ospitata nel suo prestigioso laboratorio a Leuven e per aver condiviso con me le sue importanti conoscenze scientifiche.

Al Dr. Mario di Matteo, un grazie per il costante e quotidiano confronto e supporto, nonché per tutte le "conferme" durante la mia permanenza a Leuven.

Un ringraziamento speciale a Silvia, spalla e complice senza la quale non avrei un ricordo così bello del mio periodo belga.

A Sarah, Gerlanda, Rosa, Jens, Federico e tutti gli amici e colleghi di Leuven. Grazie a voi il cielo grigio del nord non mi ha fatto rimpiangere troppo la mia Sardegna. Leuven rimarrà sempre nel mio cuore.

A Pia, una sorella maggiore alla quale riferirmi nei momenti di bisogno. Grazie per tutti i consigli e per aver sempre avuto una parola di conforto anche nei momenti più difficili.

A Simona, Claudia, Lavinia, Sandra ed a tutti i colleghi che hanno condiviso con me questi tre anni, per le risate, per i momenti belli e per quelli un po' meno belli che costellano la vita del dottorando.

A Massimo e Nicola per gli scherzi, le risate, i caffè e le palline di carta.

Ultimo, ma non per importanza, uno speciale ringraziamento ai miei genitori, a mia sorella e a Gioele, sempre al mio fianco.

# TABLE OF CONTENTS

# ABSTRACT - English

Hepatocellular carcinoma (HCC), as well as many other solid tumors, is a multi-step process whereby abnormally proliferating cancer cells undergo a large metabolic reprogramming. Mounting evidence suggests that the different metabolic alterations taking place in hepatocarcinogenesis are dependent on the activation of specific oncogenes, thus partially explaining the HCC heterogeneity. In this respect c-Myc oncogene overexpression frequently observed in human HCCs, leads to a metabolic rewiring toward a Warburg phenotype by which cancer cells avidly take up glucose and generate large volumes of lactate, through lactate dehydrogenase A (Ldha), even in the presence of oxygen. Ldha overexpression caused by boosted glycolysis is associated with poor prognosis since it results in an excess of lactate release from the neoplastic cell leading to the acidification of the extracellular space, thus favoring the emergence of an immune-permissive tumor microenvironment (TME).

In the present study we characterized the metabolic reprogramming occurring in tumors induced by the concomitant expression of c-Myc and h-Ras, two of the most frequently upregulated oncogenes in human HCCs. Using the same experimental model we also investigated effect of *Ldha* inhibition – gained through the inducible and hepatocyte-specific *Ldha* knock-down - on cancer cell metabolic reprogramming, as well as on TME alterations.

The present work revealed that c-Myc/h-Ras driven tumors display a striking glycolytic metabolism suggestive of a switch to a Warburg phenotype, and an enhanced activity of pentose phosphate pathway (PPP). However, differently from HCCs generated by the overexpression of c-Myc alone, glutamine is used to sustain glutathione synthesis instead of Tricarboxylic acid cycle (TCA) and oxidative phosphorylation (OXPHOS) is impaired.

Our results also demonstrated that *Ldha* abrogation hampers tumor growth by partially inhibiting the Warburg-like metabolic feature. In addition, loss of *Ldha* causes a remarkable increase of $Cd4^{+}$ lymphocytes compared to *Ldha* wild type livers, thus preserving the anti-neoplastic effect exerted by the CD4+ lymphocytes.

Taken together, these results suggest the potential usefulness of targeting Ldha in combination with immunotherapy to enhance the efficacy of the current therapeutic options.

# ABSTRACT - Italiano

Il carcinoma epatocellulare (HCC), così come altri tumori solidi, è un processo multi-fasico nel quale le cellule neoplastiche vanno incontro ad una consistente riprogrammazione metabolica.

Numerose evidenze suggeriscono che le differenze nelle alterazioni metaboliche che caratterizzano l'HCC siano attribuibili all'attivazione di specifici oncogeni spiegando quindi, almeno parzialmente, l'eterogeneità propria dell'HCC. A tal proposito, l'iper-espressione dell'oncogene c-Myc, frequentemente osservata nell'HCC umano, determina una riprogrammazione metabolica verso un fenotipo Warburg, tramite il quale le cellule tumorali prendono avidamente il glucosio e generano grandi quantità di lattato, mediante l'azione dell'enzima lattato deidrogenasi A (Ldha), anche in presenza di ossigeno. L'iper-espressione della Ldha, causata da una aumentata glicolisi, è associata a prognosi infausta dal momento che porta ad un rilascio eccessivo di lattato da parte delle cellule tumorali, inducendo l'acidificazione dello spazio extracellulare e favorendo l'emergenza di un microambiente tumorale (TME) immuno-permissivo.

La presente tesi ha avuto come primo obiettivo lo studio della riprogrammazione metabolica in tumori indotti dalla concomitante espressione di c-Myc e h-Ras, due tra gli oncogeni più frequentemente iper-espressi nell'HCC umano. Usando lo stesso modello sperimentale, abbiamo anche valutato l'effetto dell'inibizione della *Ldha* - ottenuto tramite una tecnica di "*Ldha* knock-down inducibile ed epatocita-specifico" - sulla riprogrammazione metabolica delle cellule tumorali e sulle alterazioni del TME.

I risultati ottenuti hanno rivelato che i tumori c-Myc/h-Ras sono caratterizzati da un forte metabolismo glicolitico indirizzato verso il fenotipo Warburg, e da un'aumentata attività della via del pentosio fosfato (PPP). Tuttavia, al contrario di quando osservato negli HCC generati dalla sola iper-espressione di c-Myc, la glutammina non viene utilizzata per rifornire

il ciclo degli acidi tricarbossilici (TCA) ma per sostenere la sintesi di glutatione. Parallelamente, si assiste ad una parziale inibizione della fosforilazione ossidativa (OXPHOS).

I nostri risultati hanno anche dimostrato che l'abrogazione della *Ldha* ostacola lo sviluppo e la progressione tumorale, tramite la parziale inibizione del metabolismo Warburg. Inoltre, la perdita della *Ldha* causa un notevole incremento dei linfociti $Cd4^+$ nel TME, rispetto a quanto osservato negli *Ldha* WT, preservando così l'effetto anti-neoplastico esercitato da questa popolazione linfocitaria

Nel complesso, questi risultati suggeriscono che la combinazione dell'immunoterapia con l'inibizione farmacologica della *Ldha* possa contribuire ad aumentare l'efficacia delle opzioni terapeutiche attualmente disponibili.

# ABBREVIATIONS

| | |
|---|---|
| Aco1/2 | Aconitase gene family |
| AFB1 | Aflatoxin B1 |
| AKT | Protein Kinase B |
| ATP | Adenosine triphosphate |
| ATPase | Adenosine triphosphatase |
| C57BL/6 | C57 black 6 mice |
| CAFs | Cancer Associated Fibroblasts |
| Casp3 | Caspase 3 |
| Cd206 | Cluster of differentiation 206; |
| DAPI | 4',6-diamidino-2-phenylindole |
| FACS | Flow cytometric analysis |
| Fbp1 | Fructose 1,6-biphosphate |
| G6pase | Glucose-6-phosphatase |
| G6pd | Glucose-6-phosphate dehydrogenase |
| Gclc | Glutamate—cysteine ligase catalytic subunit |
| Gck | Glucokinase |
| GEM | Genetically engineered mouse |
| Gls | Glutaminase |
| Glud1 | Glutamate dehydrogenase 1 |
| Glul | Glutamine synthase |
| Glut1 | Glucose transporter 1 |
| H-Ras | Harvey rat sarcoma viral oncogene homolog |
| HBV | Hepatitis B virus |
| HCV | Hepatitis C virus |
| HCC | Hepatocellular carcinoma |
| Hk2 | Hexokinase 2 |
| KD | Knock-down |
| α-Kg | α-ketoglutarate |
| Ldha | Lactate dehydrogenase a |
| Ldhb | Lactate dehydrogenase b |
| LMD | Laser-capture microdissection |
| Ly6g | Lymphocyte antigen 6 complex locus G6D; |
| Mct4 | Monocarboxylate transporter 4 |
| Mhc-II | Class II major histocompatibility complex |
| OXPHOS | Oxidative phosphorylation |
| NADPH | Nicotinamide Adenine Dinucleotide Phosphate |
| NBT | Nitro blu tetrazolium |
| Nqo1 | NAD(P)H Quinone Dehydrogenase 1 |
| Nrf2 | Nuclear factor erythroid 2-related factor 2 |
| Pd-1 | Programmed death-1 |
| Pepck1 | Phosphoenolpyruvate carboxykinases 1 |
| Pepck2 | Phosphoenolpyruvate carboxykinases 2 |
| PPP | Pentose phosphate pathway |
| qRT-PCR | Quantitative Reverse Transcription Polymerase Chain Reaction |
| ROS | Reactive oxygen species |
| RT-PCR | Reverse Transcription Polymerase Chain Reaction |
| Ras | Rat Sarcoma |
| SB | Sleeping Beauty |
| Sdha | Succinate dehydrogenase subunit A |

| | |
|---|---|
| Slc1a5 | Glutamine transporter |
| Tet | Tetracycline |
| TCA | Tricarboxylic Acids |
| TME | Tumor microenvironment |
| Vegf | Vascular endothelial growth factor. |
| WT | Wild-type |

# INTRODUCTION

## Metabolic reprogramming as a hallmark of cancer

Cancer is the result of a multistep process in which malignant transformation requires the elimination of several cell-imposed barriers such as anti-proliferative responses, programmed cell death, and senescence. These cancer-associated features have been deeply investigated leading to the identification of so-called “hallmarks of cancer” (1).

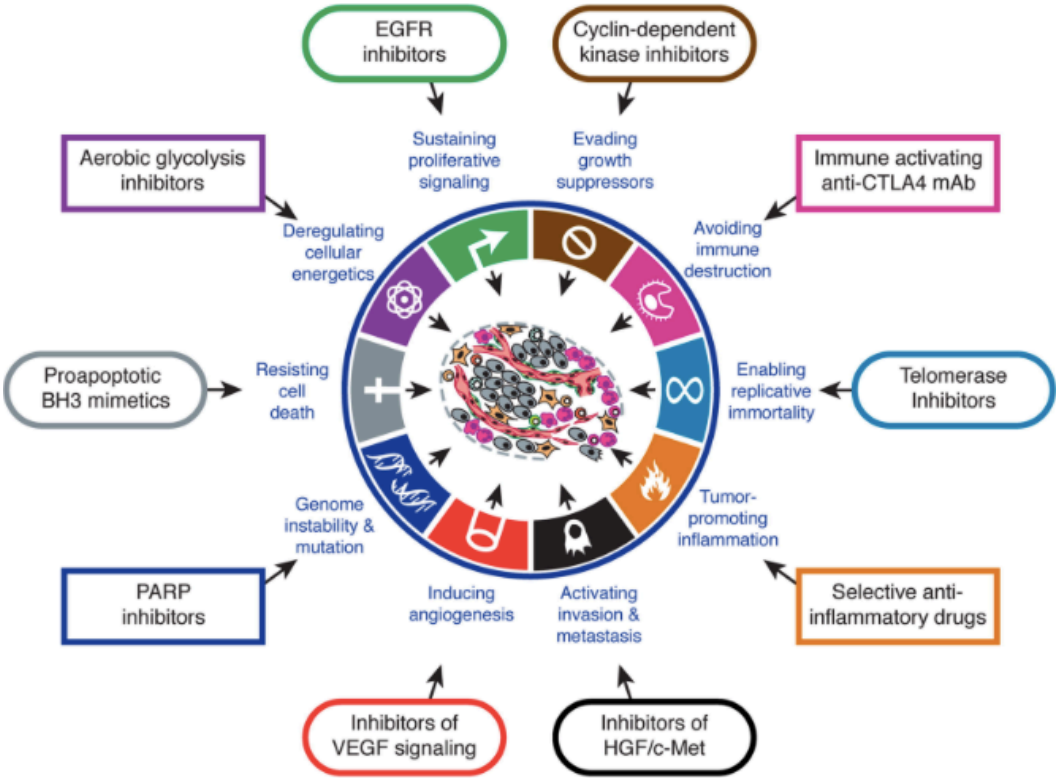


**Figure 1. The hallmarks of Cancer (2).**

Following the original 2000 review by Hanahan and Weinberg, further studies made over the past years in cancer research led to revisit and include new hallmarks (2) (Fig. 1). Overall, the fundamental work of these scientists paved the way to develop new therapeutic approaches. Indeed, drugs that interfere with some of the ‘hallmarks of cancer’ have been already generated, used in clinical trials, and some of them approved for clinical use.

Among the several hallmarks of cancer, metabolic reprogramming is considered to be a critical process as it is needed to enhance cell proliferation and survival. More in detail, cancer cells acquire the ability to gain necessary nutrients, exploiting them in metabolic pathways that contribute to tumorigenesis. This cellular metabolic reprogramming is both direct and indirect consequence of oncogenic mutations and is a main actor in the maintenance of the tumorigenic state (3).

## Warburg effect

Although interest in altered cancer metabolism has been renewed in the last decade, the first observations on metabolic reprogramming of cancer cells were made almost a century ago by the German physiologist Otto Warburg. In most mammalian cells, glucose is metabolized through glycolysis in a multistep set of reactions resulting in the production of pyruvate. Under normal oxygen levels, in normal cells the majority of pyruvate enters the mitochondria to generate the energy needed for cellular processes. Warburg theory outlined how cancer cells preferentially rely on so-called “aerobic glycolysis”, in which much of the pyruvate from glycolysis is redirected to generate lactate through the action of lactate dehydrogenase (Ldha)—a process typically observed in conditions of low oxygen state (4).

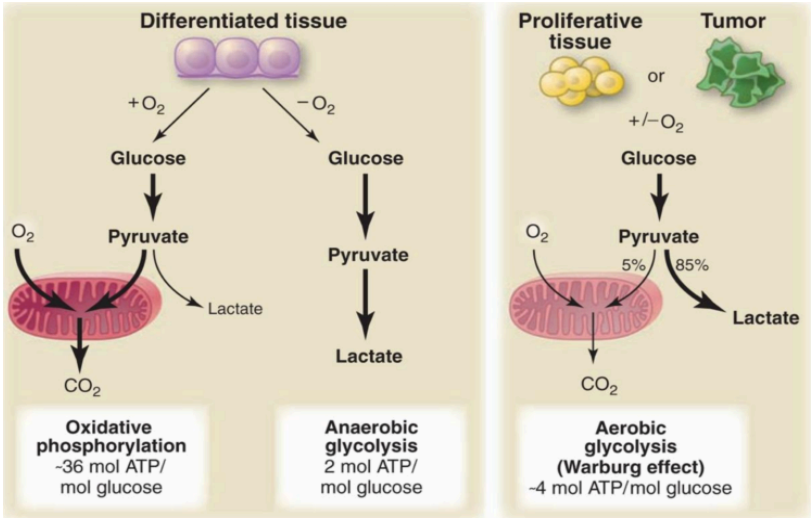


**Figure 2. Schematic representation of glucose metabolism in normal and cancer cells (4).**

A first explanation for Warburg's observation was that cancer cells develop mitochondrial defects that impair aerobic respiration thus leading the cells to rely on glycolysis for energy production (5–7). However, this hypothesis was refuted by several works reporting that mitochondrial function is not necessarily impaired in most cancer cells. Taken together, these contrasting findings suggest that the activation of glycolysis in the presence of normal oxygen values may be influenced by the tumor microenvironment or by specific genetic alterations, making this issue still controversial (8,9). Nevertheless, among possible explanations for the abovementioned metabolic reprogramming, it was proposed that inefficient ATP production constitutes an obstacle only when poor supply of nutrients occurs. Cancer cells are not affected by this deficient ATP production since they can rely on a strong up-regulation of glucose transporters, leading to increased glucose uptake (10). In fact, the majority of cancer cells display a glycolytic activity that is estimated to be even 200-fold higher than that of normal cells (11). Therefore, increased supply of glucose, along with a high rate of glycolytic activity, leads to an increased ATP production even in conditions of normal oxygen levels. Another possible reason is that the high proliferative rate of cancer cells not only requires enhanced ATP production, but also needs nucleotides, amino acids and lipids in order to sustain cell growth. Indeed, in normal conditions 36 ATP molecules are generated by oxidative phosphorylation (OXPHOS) with only 2 Nicotinamide Adenine Dinucleotide Phosphate (NADPH) through the Pentose Phosphate Pathway (PPP) and 6 carbons. However, cancer cell need more equivalents of carbon to produce amino acids and nucleotides and to build the molecular skeleton; they also need NADPH as a reducing equivalent for a variety of biosynthetic reactions, and to maintain cellular redox capacity. While the tricarboxylic Acid Cycle (TCA cycle) can be utilized for fatty acid synthesis, glycolysis intermediates can be useful also for aminoacid biosynthesis and ribose for nucleotides (4). To satisfy their demand, many tumors down-regulate mitochondrial respiration in favor of aerobic glycolysis. Indeed, by converting all the glucose to CO2 via

OXPHOS and maximizing ATP production, cells would lose the required carbons. OXPHOS generate also reactive oxygen species (ROS) that can be deleterious for cancer cell survival, and in addition, the TCA cycle exerts a negative regulation on glucose metabolism. By preferentially converting glucose into lactate, cancer cells prevent the feedback repression of glycolysis by the excess of mitochondrial ATP (3).

## Role of Lactate in promoting tumorigenesis

As mentioned above, the Warburg effect implies that tumor cells uptake large amounts of glucose thus producing increase of lactate, even in the presence of oxygen. The high amount of glucose that proceeds along glycolysis ultimately produces two molecules of pyruvate, which is preferentially converted into lactate by the upregulation of the enzymes lactate dehydrogenases (Ldh). Lactate dehydrogenase is a tetrameric enzyme comprising two major subunits, A and B. Ldha, which is the predominant form in skeletal muscle and liver, kinetically favors the conversion of pyruvate to lactate, while Ldhb, preferentially found in heart muscle, converts lactate to pyruvate that is further oxidized (12). For a long time, lactate was only recognized as a “metabolic waste product” derived from aerobic glycolysis. However, lactate recently gained a growing interest since it has been demonstrated that it can be utilized as a source of energy, can act as an oncometabolite and can boost tumor progression by promoting invasion and metastasis. Moreover, it has been reported that lactate drives the suppression of the immune-microenvironment and participates to drug resistance (13).

As a matter of fact, the consequence of lactate accumulation is an acidification of the extracellular pH in tumor microenvironment. This acidosis favors processes, such as metastasis, angiogenesis and more importantly, immunosuppression by affecting a number of cell types within the tumor microenvironment (TME) such as endothelial cells, cancer-associated fibroblasts (CAFs), immune cells and non-cancer stroma, being associated with a worse clinical prognosis (14).

Moreover, generation of lactate from pyruvate requires NADH as an electron donor; NAD+ - the product of this reaction - acts as an electron acceptor to support more glycolytic reactions. This event triggers a co-dependency between glycolysis and lactate generation, thus ensuring that glycolysis can be successfully maintained regardless of its rate, even with low oxygen concentrations. The production and excretion of lactate, an otherwise energetically wasteful activity, is actually necessary to sustain the Warburg effect as it ensures the continuous generation of $NAD^+$ to serve as an electron acceptor during glucose oxidation (15).

Thus, lactate should be thought as an important oncometabolite in the metabolic reprogramming of cancer.

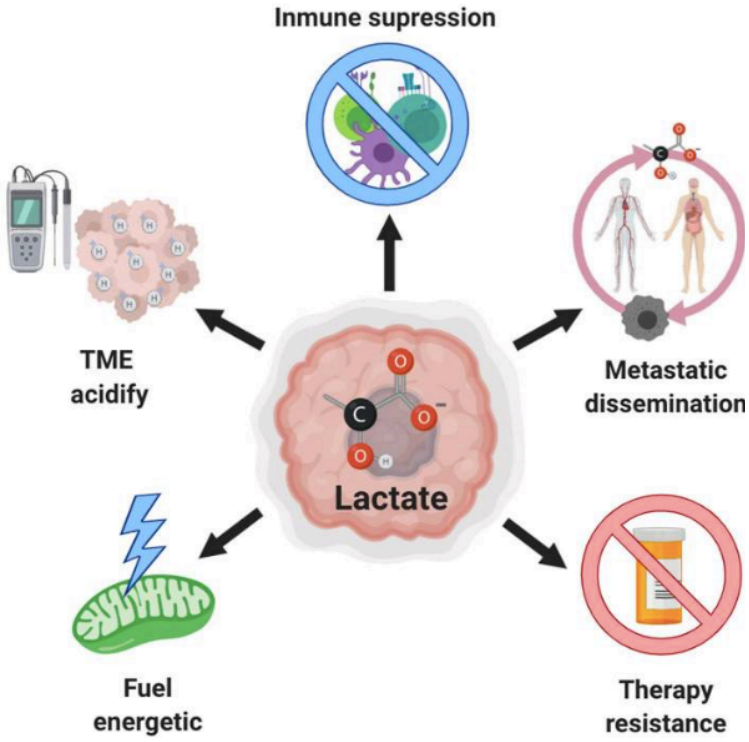


**Figure 3. Schematic representation of the pro-tumorigenic effect of lactate on tumoral microenvironment (13).**

## Oncogene-driven metabolic changes

In the last years, it has been reported that the metabolic changes observed in cancer cells can also be the consequence of a particular oncogene status. Indeed, several efforts have been made to identify the mutations that contribute to cancer initiation and progression. Recent works, demonstrated that the main metabolic alterations observed in the Warburg effect, such as increased glucose catabolism, decreased OXPHOS, and increased lactate production are also peculiar features of oncogene activation (16). For example, the powerful oncogene Rat Sarcoma (Ras) is a well-known promoter of glycolysis (17,18). In fact, the expression of the glucose transporter 1 (Glut1) was strongly upregulated in K-Ras mutated cells. The increased expression of Glut1 was associated with an increased glucose uptake, increased glycolysis and higher lactate production, whereas mitochondrial functions and OXPHOS were not affected (19). Akt kinase (protein kinase B), a well-known downstream effector of insulin signaling, boosts the uptake of glucose and its consumption in cancer (20), whereas the proto-oncogene transcription factor myelocytomatosis oncogene (c-Myc) upregulates the expression of various metabolic genes (21). Overall, a growing amount of evidences, suggests that tumorigenesis is the result of the activation of key oncogenes in order to allow cancer cells to acquire more efficient proliferative capabilities, and that metabolism may play a pivotal role in this process (16).

## Hepatocellular Carcinoma (HCC)

The above-mentioned metabolic reprogramming has been described in a variety of solid tumors, including hepatocellular carcinoma (HCC) (22–24). HCC represents the most common type of primary liver cancer (25) and it is the fourth leading-cause of cancer related death worldwide (26), constituting a significant challenge for global health. Despite an important increase in incidence, current treatment options remain unsatisfactory (27).

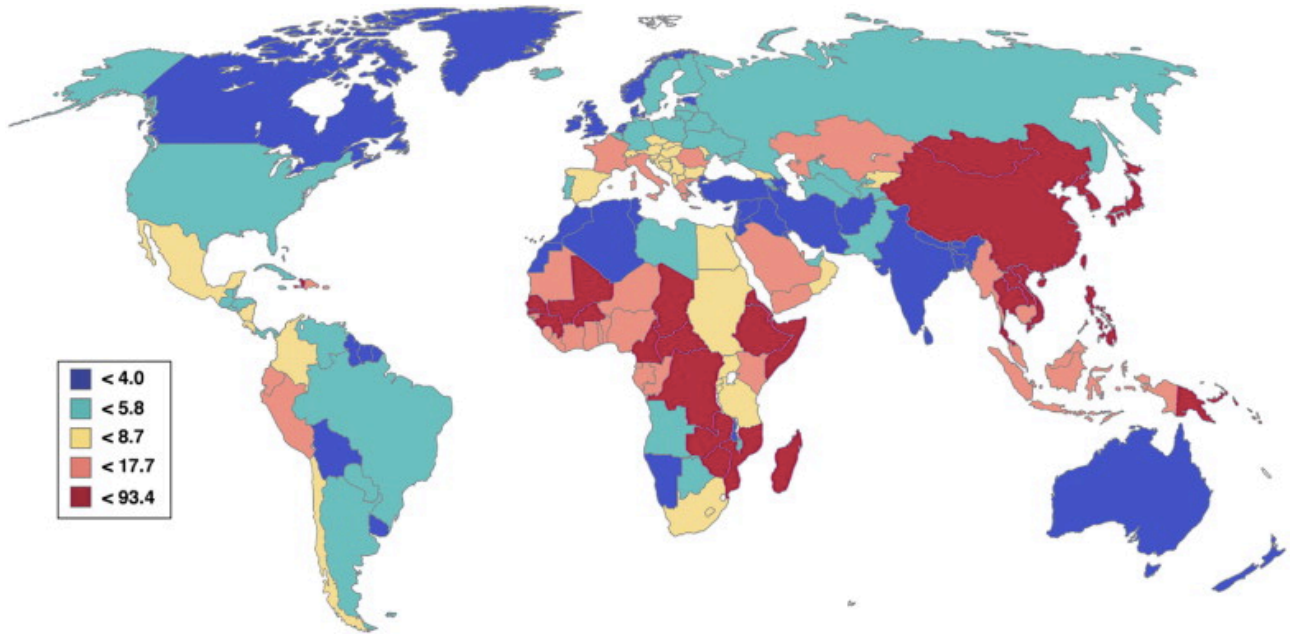


**Figure 4. Regional variation in mortality rate of HCC categorized by age adjusted mortality rate. The rate is expressed per 100.000 persons (28).**

Approximately 850,000 new liver cancer cases and 800,000 deaths are registered per year (29). Sub-Saharan Africa and Eastern Asia account for the majority of HCC cases, but more than 50% of the world's burden arise from China (28). Countries of the Central Europe exhibit intermediate incidence rates, while Northern Europe, Middle East, Oceania and America display the lowest incidence rates (30). In almost all populations, HCC is also influenced by gender and age. Indeed, males display higher liver cancer incidence compared to females, with a ratio between 2:1 and 4:1 (28).

Regions with high and low-rate incidence of HCC are characterized by a prevalence of different relevant risk factors. In high-rate regions, such as Asia and Africa, the major risk factors are characterized by Hepatitis B virus (HBV) infection and consumption of Aflatoxin B1 (AFB1)-contaminated food; while in low-rate areas the most common risk factors are represented by Hepatitis C virus (HCV) infection, alcohol consumption, obesity, diabetes and metabolic syndrome (28).

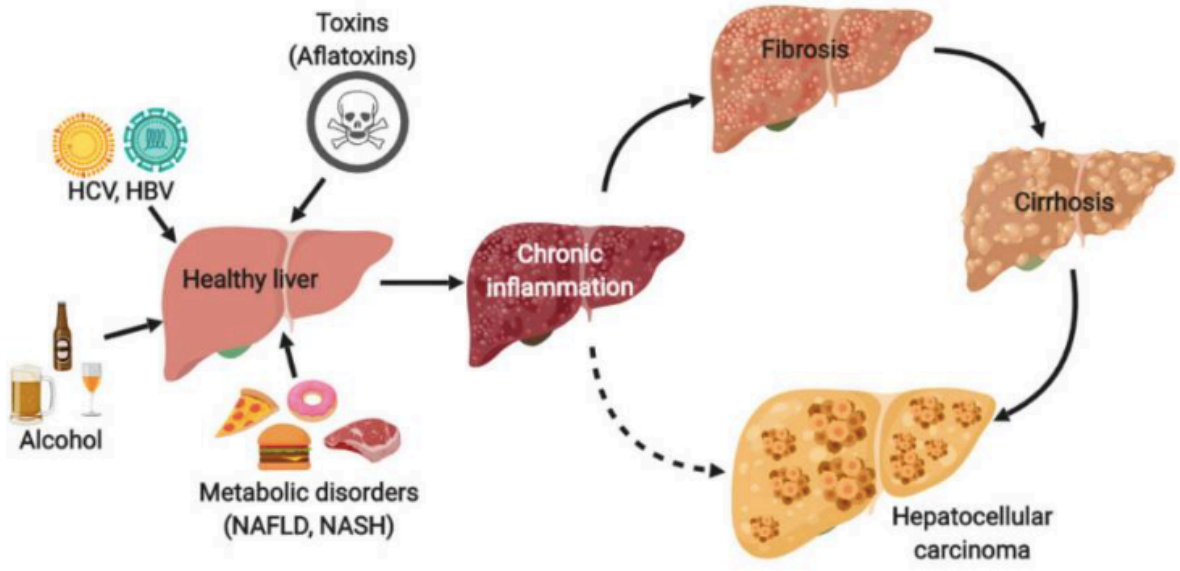


**Figure 5. Risks factor and schematic representation of the process that leads to hepatocellular carcinoma development (31).**

## Natural history of HCC

HCC development, similar to other solid tumors, is a sequential and complex multi-step process. HCC often arises from a chronic liver disease characterized by inflammation and fibrosis/cirrhosis. The necessary exposure-time for the occurrence of HCC is controversial, since observations of patients exposed to well-known risk factors for HCC show discrepancy in the window of time from the exposure to the manifestation of HCC. Studies on HCV-infected patients highlight that HCC development requires about 10 years from the diagnosis of cirrhosis and 30 from the exposure to the virus (32), while in HBV-derived HCC, the time course is less predictable, since HCC may precede the occurrence of cirrhosis (33). Unfortunately, the diagnosis of HCC is made at late stages with no effective curative treatment to improve patient's survival that in case of advanced HCC is only 0-10% (34). The multikinase inhibitor Sorafenib, the first Food and Drug Administration (FDA)-approved drug for HCC (35), showed an increased survival of only 3 months among patients exhibiting advanced- stage disease (27). More recently, Regorafenib - another multi-kinase

inhibitor - has been approved as a second-line therapy for HCC (36). Also in this case, the results were unsatisfactory, even if a recent study documented an improvement of the overall survival (37).

The absence of more effective therapeutic options highlights the need of studies aimed to identify new target pathways involved in the development of HCC, to improve the design and development of more effective compounds and the identification of new markers. Unfortunately, although HCC development is the result of a multistage process, most human HCCs are detected at very late-stages, thus making impossible to discriminate the molecular alterations that drive the tumorigenic process from those that are simply the consequence of cell transformation (23).

Since studies on initial HCC stages in humans are hampered by the clinical difficulty of diagnosing early lesions, experimental models that allow to dissect the several steps of HCC are mandatory.

## HCC animal models: Genetically Engineered Mouse Models

Gene expression profile performed in several HCC cell lines established that they only partially recapitulate the expression pattern of human HCC tissue-derived metabolic genes (38). Indeed, in spite of the impressive number of studies on HCC metabolic reprogramming performed using cancer cell lines, it is clear that they cannot reproduce the complexity of primary tumors for at least two reasons: 1) continuous culturing of cancer cells leads to the introduction of genetic mutations not represented in the original tumors; moreover, the *in-vitro* culture system is not able to satisfactorily summarize the *in-vivo* metabolic cross-talk between HCCs and the tumor microenvironment; 2) hepatocarcinogenesis is a multi-step process and the employment of cancer cell lines does not permit to distinguish the metabolic changes that are a consequence of cell neoplastic

transformation from the ones that drive the tumorigenic process. Thus, the identification of animal models allowing to discriminate the several step of HCCs became mandatory (39). A variety of rodent animal models that allow to study of the metabolic changes that take parts in HCC development is currently available (40). Among them, murine models of HCC, such as chemically-induced models, xenograft models, and genetically engineered mouse (GEM) models, are considered effective tools to reproduce, at least in part, human HCC pathology (39,41)

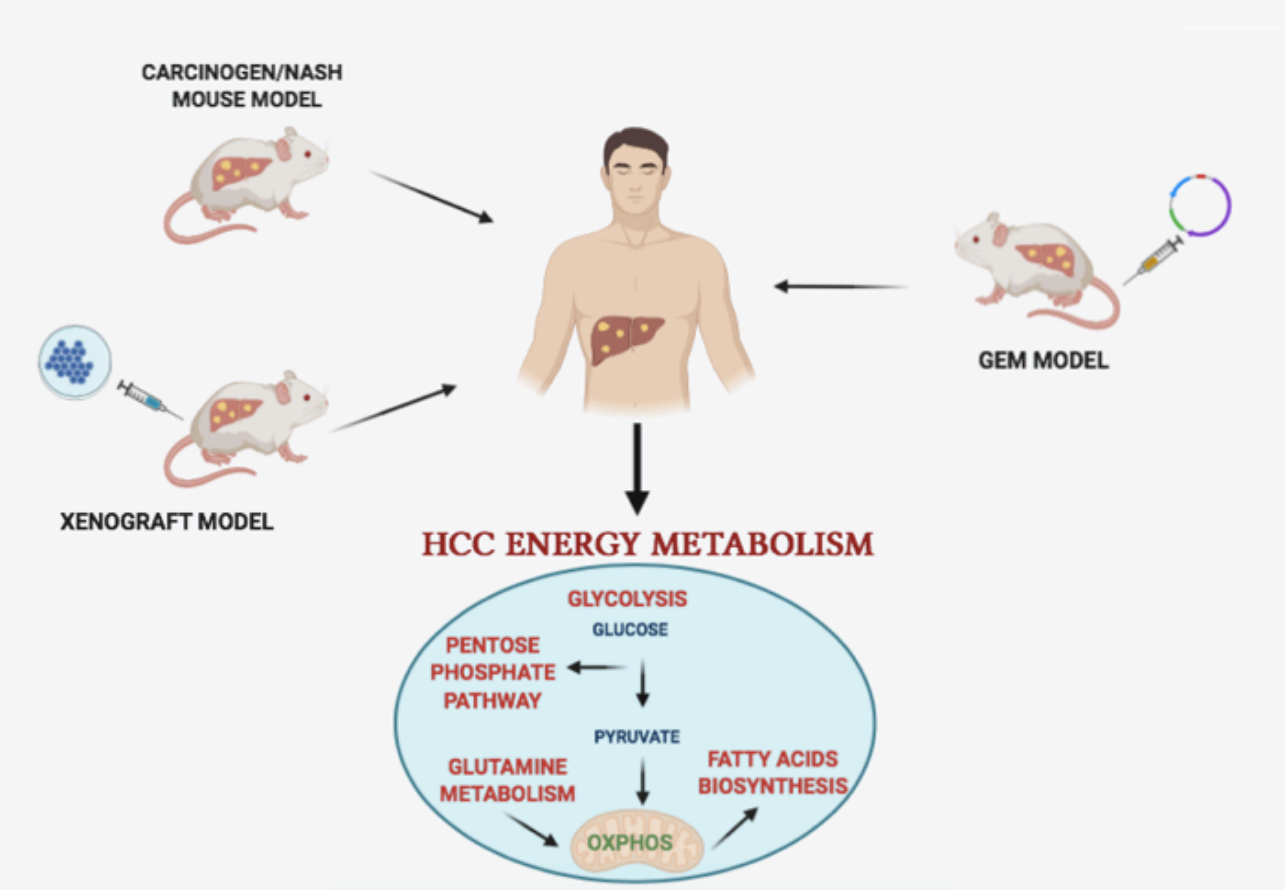


**Figure 6. Animal models used to study HCC metabolic reprogramming. Slightly adapted from Serra et al. (39).**

Animal models consisting of chemically-induced HCC have been largely used in cancer research. These models allow to dissect the several steps of multistage hepatocarcinogenesis, and by combining the carcinogen with toxicants like alcohol, carbon tetrachloride, or Western diet, they may often generate chronic insults observed in human HCC, such as injury, inflammation, and fibrosis. On the other hand, an important disadvantage of chemically induced models is the requirement of a long time to induce tumorigenesis as well as the notion that besides rare exceptions (i.e. Aflatoxin), no chemical carcinogens have been convincingly associated to human HCC.

Recently, GEM models have been preferred for studying the metabolic alterations that occur in human disease since they quickly and greatly recapitulate human genetic and pathophysiological alterations (42).

In this context, systems that allow temporal control of target gene expression, such as the tamoxifen-regulated Cre-loxP and the tetracycline (Tet) regulatory systems, are more suitable to study the metabolic alterations underlying HCC pathogenesis. In the Cre-loxP system, the expression of a gene of interest can be induced with a tamoxifen treatment. In normal condition, the Cre-estrogen receptor fusion protein (Cre-ER) remains in the cytosol. However, in response to tamoxifen treatment - usually introduced via an intraperitoneal injection - Cre-ER translocates into the nucleus inducing the recombination between the loxP sites, thus resulting in the control of expression of the target gene. This system has enabled researchers to investigate genes of interest in a tissue/cell (spatial control) and/or time (temporal control) specific manner (43,44).

## Hydrodynamic Injection

Recently, a liver-specific transgenic approach was developed to generate a powerful murine model for liver cancer research. This method that employs the Sleeping Beauty (SB) transposase system and the hydrodynamics-based transfection has become a very efficient

tool to study the pathogenesis of liver cancer (41,45). The SB transposase mediates chromosomal integration of transposons for long-term expression of genes located between specific repeating sequences (IRs) and carried by plasmids, in hepatocytes.

The hydrodynamic transfection utilized the force produced by the injection of a large volume of DNA plasmid solution into the blood vessel, causing the permeabilization of the capillary endothelium and generating pores in the plasma membrane of the surrounding parenchyma cells, thus providing DNA access. Subsequently, the DNA trapped inside the parenchymal cells due to the closure of the pores of the plasma membrane.

This approach originally developed by Liu et al. (46) consists of a rapid tail vein injection (5 to 9 seconds) of DNA plasmid, diluted in a saline solution volume, equivalent to 10% of body weight. The injection of this large volume of DNA solution directly into the inferior vena cava induces cardiac congestion, delivering the injected solution into the liver in a retrograde manner, leading to a very successful gene delivery into mouse hepatocytes.

Liver is the organ with the greater uptake of plasmid DNA in the body, with a successful hepatocyte transfection rate of approximately 10% to 40% (45).

## HCC metabolic reprogramming

The liver is the organ responsible for most metabolic processes, such as detoxification of endogenous/exogenous substances, glucose storage in the form of glycogen, and the synthesis of aminoacid precursors to produce proteins. Hepatocytes represent the great majority of the total mass of the liver (47), and are responsible for most metabolic processes. Due to the fundamental role of hepatocytes in liver metabolism, it is not surprising that HCC is, by enlarge, the most represented tumor of this organ being characterized by a profound dysregulation of metabolic processes that can sustain tumorigenesis (23,48,49).

Identification of alterations that distinguish HCC from normal liver might result extremely helpful in identifying new targets for the therapy of this lethal tumor (23). With this aim, several studies revealed that metabolic gene networks are heterogenous in all type of cancers, including HCC (50). However, a study by Nwosu et al. (23) regarding the expression of 2761 metabolic genes in 521 human HCC identified several deregulated metabolic genes regardless of the etiological background of the different groups of patients. Among these genes, those involved in glycolysis, PPP, TCA cycle, nucleotides biosynthesis, lipid and glutamine transporters were the most dysregulated. In detail, as mentioned before, one of the key signature of the Warburg effect characterizing metabolic reprogramming that occurs during hepato-carcinogenesis is an increased glucose uptake and lactate production even in normal oxygen conditions and fully functioning mitochondria (3,51). However, this event is not correlated with enhanced gluconeogenesis as the expression levels of phosphoenolpyruvate carboxykinases 1 and 2 (Pepck1 and 2) and fructose 1,6-bisphosphatase 1 (Fbp1), are downregulated in HCC (52). The increased glucose uptake by cancer cells is mediated by the upregulation of glucose transporter 1 (Glut1), by which glucose enters the cancer cell and it is mainly used in the glycolytic pathway (53–55). Once inside the cell, the excess of glucose is converted to glucose-6-phosphate (G6p) through the upregulation of Hexokinase 2 (Hk2), which is the pro-tumorigenic isoform of the first glycolytic enzyme glucokinase (Gck). A considerable part of G6p is redirected into the Pentose Phosphate Pathway (PPP) through the enhanced activity of glucose-6-phosphate dehydrogenase (G6pd), that provides nucleotides and NADPH (56). Other glycolytic intermediates proceed along glycolysis leading to lactate production that requires the overexpression of lactate dehydrogenase A (Ldha) (57,58). Excess of lactate is exported in the tumor microenvironment mainly throughout the upregulation of monocarboxylate transporter 4 (Mct4) (59).

Another important component of metabolic reprogramming is glutamine, an α-amino acid used in the biosynthesis of proteins. It has been shown that glutamine is also involved in lipid synthesis after its conversion into glutamate by mitochondrial glutaminases (Gls). Glutamate is then converted into α-ketoglutarate (αKG) which can enter the TCA cycle, or, alternatively, αKG can undergo a reductive carboxylation by which is transformed in citrate (60,61).

The role of TCA cycle and OXPHOS in HCC remains still a controversial topic. Kowalik et al. demonstrated the impairment of Succinate dehydrogenase complex A (Sdha) activity since the very initial steps of HCC development (56). Importantly, SDHA not only converts the succinate into fumarate but also represents the complex II of the respiratory chain, since early HCC stages. On the other hand, other studies reported that most of the TCA cycle genes and corresponding intermediates are up-regulated in tumor cells, except for the down-regulation of the aconitase gene family (Aco1/2), suggesting the TCA cycle is at least partially activated (61).

## C-MyC driven HCC metabolic reprogramming

Recently, the role of the proto-oncogene c-Myc in tumor development and progression aroused a lot of interest since many of the metabolic changes occurring in transformed cells are driven by its overexpression. The transcription factor proto-oncogene c-Myc is a pleiotropic transcription factor and is one of the most common genes found to be overexpressed in human cancers (62). As an immediate early gene, c-Myc is considered to be a key factor in the transcriptional response that leads to the transition of hepatocytes from G0/G1 to the S phase(63,64). Accordingly, c-Myc has been found strongly up-regulated in hepatocyte proliferation that occurs during liver regeneration (65).

In HCC, Myc is frequently overexpressed and associated with aggressiveness and poor prognosis (66–71). Furthermore, c-Myc boosts glucose uptake (72,73) and its catabolism to

lactate, as well as it promotes glutaminolysis to fuel the TCA cycle. Indeed, the authors found the concomitant upregulation of Ldha and Hk2, the pro-tumorigenic isoform of the first glycolytic enzyme Gck. With regard to glutamine pathway, c-Myc promotes glutaminolysis by increasing the expression of the glutamine transporter Slc1a5 (72,74) and by promoting the expression of Gls, the enzyme responsible of its catabolism, while the expression of Glul, the gene coding for glutamine synthase, was diminished. Moreover, in a C-Myc driven model of HCC, it has been demonstrated that glutamine-derived carbons are preferentially redirected into the TCA cycle, assessed by the downregulation of Gclc, the enzyme which converts glutamate into glutathione (75).

# AIM OF THE STUDY

Cancer metabolic reprogramming is considered to play a critical role in cancer development, including Hepatocellular Carcinoma (HCC). It is generally believed that a strong dysregulation of energy metabolism leads to enhanced glucose uptake independently of oxygen availability. This metabolic switch results in excessive lactate production which, after cellular extrusion, leads to acidification of the extracellular environment contributing to tumor development.

However, contrasting results have been obtained depending on the adopted experimental model. In particular, it has been suggested that different oncogenes may lead to different metabolic alterations of HCC.

Based on this premise, the aim of the present study can be summarized as follows:

- Characterizing the metabolic alterations occurring in mouse HCC generated by co-transfection of c-Myc and h-Ras$^{G12}$ oncogenes, frequently overexpressed in human Hepatocellular carcinoma (70,71,76,77).
- Investigating the role of Lactate Dehydrogenase A (Ldha) - the enzyme responsible of the conversion of pyruvate into lactate - in a conditional hepatocyte-specific KO mouse model of c-Myc/h-Ras driven hepatocarcinogenesis.

# MATERIAL AND METHODS

## Animals

Ldha$^{lox/lox}$ cKO male mice in a C57BL/6 background were kindly provided by Prof. David Scadden (Harvard Stem Cell Institute - HSCI), while C57BL/6 WT mice were purchased form Charles River Laboratories (Bruxelles, Belgium). Animals have been fed with a rodent standard diet and maintained at 25°C temperature and 12 hours light/dark daily cycle, with food and water ad libitum. Housing and all experimental animal procedures were approved by the Institutional Animal Care and Research Advisory Committee of KU Leuven.

## Experimental Protocol 1


**Figure 7. Schematic representation of experimental protocol 1**

Six-eight weeks old C57BL/6 male mice were hydrodynamically co-transfected with 0.1 μg of PB_h-Ras$^{G12V}$ and PB_c-Myc, in conjunction with a plasmid encoding a hyperactive PB transposase (hyPBase). The liver-specific promoter minimal transthyretin (TTRmin) was used to drive gene expression in all PB constructs. Tumor bearing mice were sacrificed 14 weeks after hydrodynamic injection. (Fig. 7)

## Experimental Protocol 2

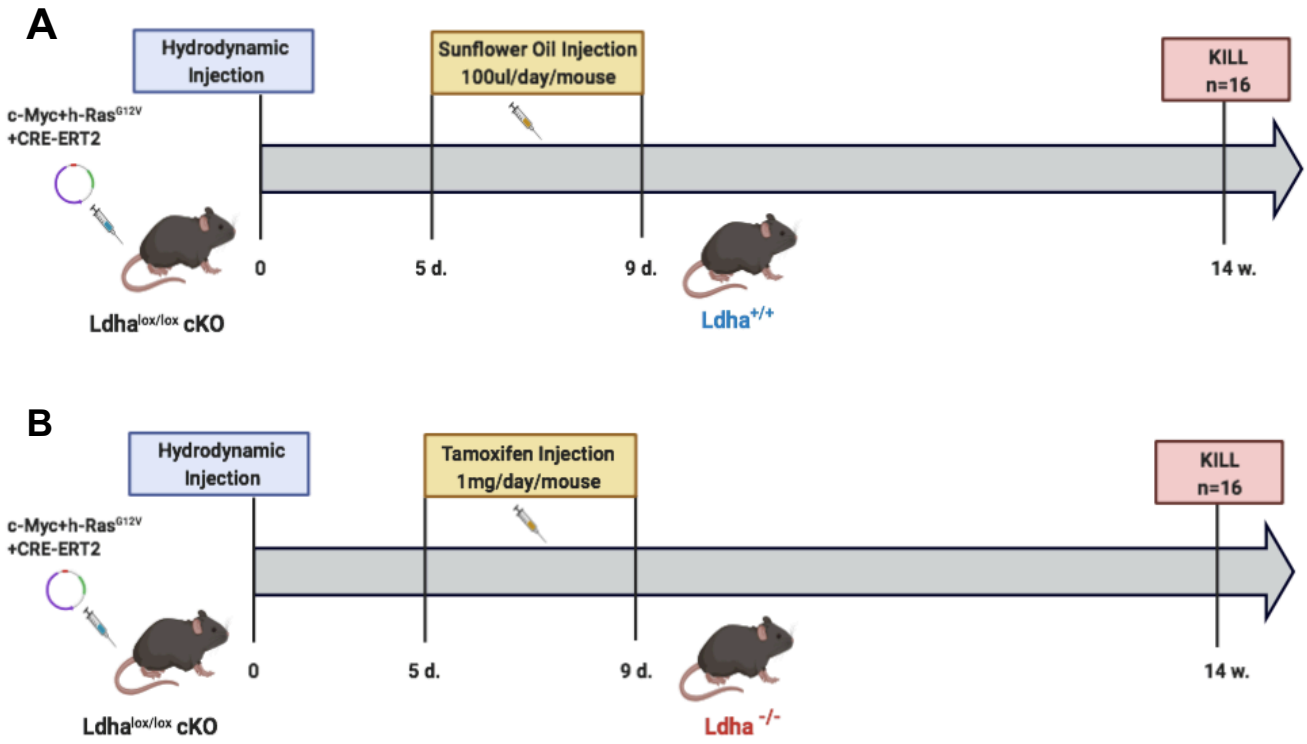


**Figure 8. Schematic representation of experimental protocol 2**

Six-eight weeks old Ldha$^{lox/lox}$ cKO male mice in a C57BL/6 background were hydrodynamically co-transfected with 0.1 μg of PB_h-Ras$^{G12V}$, PB_c-Myc and PB_CRE_ERT2, in conjunction with a plasmid encoding a hyperactive PB transposase (hyPBase). The liver-specific promoter minimal transthyretin (TTRmin) was used to drive gene expression in all PB constructs. 5 days after hydrodynamic injection mice were subjected to A) intra-peritoneal tamoxifen injection (1 mg/day/mouse) or B) intra-peritoneal corn oil injection (100 μL/mouse/day) resulting in Ldha$^{+/+}$ and Ldha $^{-/-}$ mice, respectively. 14 weeks after hydrodynamic injection tumor bearing mice from both groups were sacrificed (Fig. 8).

## Tamoxifen administration

30 mg of Tamoxifen (Sigma - Aldrich, T5648) were dissolved in 125 µL of 100% Ethanol together with 875 µL of Sunflower seed oil (Santa Cruz, sc-215936) and mixed well by vortexing for at least 30 min. at room temperature. The obtained 30 mg/ml Tamoxifen solution was then diluted 1:3 with additional Sunflower seed oil to obtain the concentration of 10 mg/ml. 100 µL of this final working solution were administered via intraperitoneal injection consecutively every 24 hours for 5 days.

## Histology and immunohistochemistry

### *Tissue preservation*

Immediately after the sacrifice, livers were cut into several pieces. For immunohistochemistry, liver sections were fixed in 10% formalin, embedded in paraffin and stored at room temperature (RT). Other sections were immediately frozen using Optimal Cutting Temperature (OCT) and preserved at -80°C for future molecular analysis and cryo-sectioning.

### *Hematoxylin and Eosin (H&E) staining*

Four micron-thick paraffin-embedded liver sections were de-paraffinized in Bioclear solution (Bio-Optica, Milan, Italy) for 30 minutes and hydrated in a decreasing alcholo-scale. Sections were then incubated in Carazzi Hematoxylin for 20 minutes and after several washes in tap water, stained in 1% acidified alcoholic eosin for 12 seconds. Sections were then dehydrated through ascending alcohol series, cleared with Bioclear, air-dried and then mounted using synthetic mounting and cover-slipped.

***C-Myc, Ki-67, G6pd, Glul, Gls, β-catenin, Caspase 3 staining***

Four micron-thick sections were deparaffinized in BioClear for 1 hour and rehydrated in decreasing series of alcohol. Following two washes in PBS, antigen retrieval in Sodium Citrate Buffer was performed. A detailed description of primary and secondary antibody dilutions is described in Table 1.

**Table 1. List of antibodies for IHC**

| Staining | Retrieval Conditions | Primary antibody | Secondary antibody |
|---|---|---|---|
| C-Myc | 3x5 MWO 700W. Sodium Citrate | 1:100 ab32072 O/N 4°C | Dako anti-rabbit 45 min. RT |
| Ki-67 | 2x5 MWO 700W Sodium Citrate | 1:300 ab15580 O/N 4°C | Dako anti-rabbit 45 min. RT |
| G6pd | 2x5 MWO 700W Sodium Citrate | 1:100 ab 87230 O/N 4°C | Dako anti-rabbit 45 min. RT |
| Glul | NO | 1:1000 Sigma G2781 O/N 4°C | Dako anti-rabbit 45 min. RT |
| Gls | 3x5 MWO 700W EDTA | 1:200 ab 262716 G2781 O/N 4°C | Dako anti-rabbit 45 min. RT |
| ß-catenin | 6x5 MWO 700W Sodium Citrate | 1:50 ab32572 O/N 4°C | Biotinylated anti-rabbit 1:300 30 min RT + Vectastain Elite ABC HRP Kit 30 min. |
| Cleaved Casp-3 | 5x5 MWO 700W Sodium Citrate | 1:50 Cell Sign 9664L O/N 4°C | Biotinylated anti-rabbit 1:200 30 min RT + Vectastain Elite ABC HRP Kit 30 min. |

***Complex II/Succinate Dehydrogenase (Sdh) histochemical assay***

Eight micron-thick frozen sections were incubated at 37°C in incubation medium containing 0.2 M phosphate buffer, sodium succinate solution, nitro blu tetrazolium (NBT) solution (Sigma-Aldrich) and distilled water. Successively, liver sections were rinsed in physiological saline, fixed in 10% formalin-saline solution, rinsed in 15% alcohol and finally mounted with an aqueous mounting medium. As succinate was oxidized to fumarate, the reduced form of NADH was produced and the reaction was visualized concomitantly with the electron acceptor reacting with the purple salt NBT.

## Laser capture microdissection

Sixteen-micron-thick serial frozen sections were cut and attached to 2-µm RNase-free PEN-membrane slides (Leica, Bannockburn, IL). To identify the localization of pre-neoplastic lesions, 6 µm thick sections were cut and stained for H&E in order to recognize the HCC lesions. Immediately before performing micro-dissection, frozen sections were rapidly stained with a 3.5 minutes H&E procedure. Briefly, sections were hydrated (30 seconds in Ethanol 100% and 95%), stained in Mayer's hematoxylin for 90 seconds, washed in water for 20 seconds, stained in 0.25% alcoholic Eosin for 10 seconds and dehydrated by Ethanol 100% for 30 seconds. Micro-dissection was performed using a Leica laser microdissection apparatus (LMD6000). The whole procedure was performed within 20 minutes to avoid RNA degradation. To guarantee the maximum amount of material, the same lesion was identified and cut from 5 to 10 serial sections. Dissected material from the same nodule was collected in the same 0.5 ml micro centrifuge tube's cup filled with 50 µL of Extraction Buffer (XB). At the end of the procedure, microtubes were plugged up, incubated for 30 minutes at 42°C, centrifuged to collect dissected material and immediately frozen at -80°C until extraction with PicoPure™ RNA Isolation Kit (Applied Biosystem, KIT0204).

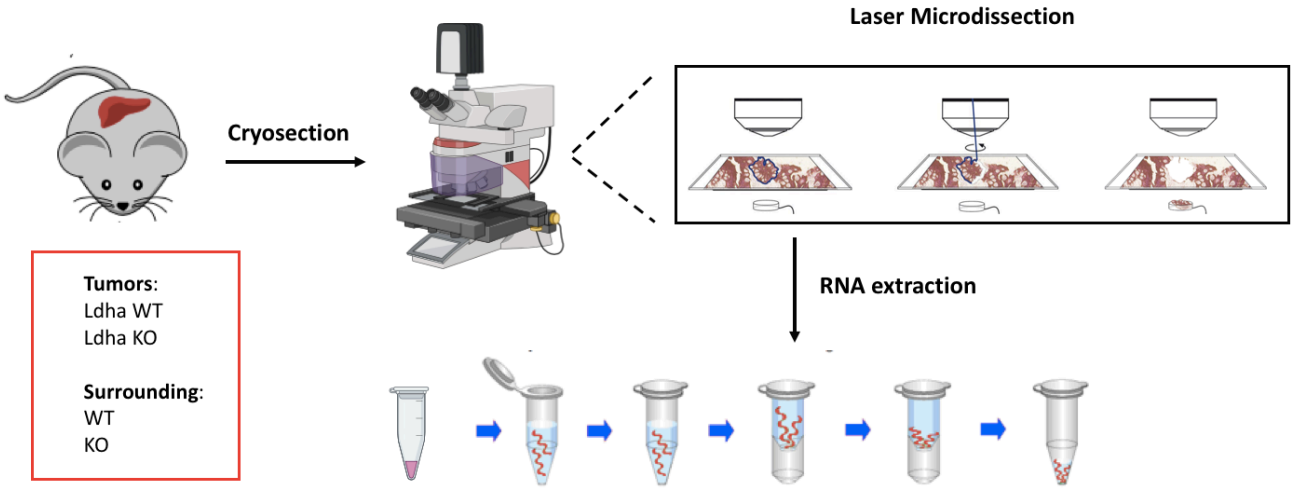


**Figure 9. Schematic Workflow of Laser Microdissection followed by RNA extraction.**

## RNA extraction

***RNA extraction from micro-dissected HCCs and surrounding livers (Cryo samples)***

PicoPure™ RNA Isolation Kit (Applied Biosystem, KIT0204) was used for the extraction of total RNA from HCCs and from the corresponding surrounding livers. Briefly, once microdissected, collected lesions were dissolved in 50 µL of Extraction Buffer (XB), heated and centrifuged as described before. Rna purification column were pre-conditioned with 250 µL of Conditioning Buffer (CB) directly into the filter membrane. Column were incubated at room temperature for 5 minutes and then centrifuged in the provided collection tube at 16,000 x g for one minute. The obtained cell extract was incubated with equal volume (50 µL) of 70% Ethanol (EtOH) and mixed well by pipetting up and down; the mix of cell extract and ethanol was then transferred into the purification column and centrifuged for 2 minutes at 100 g in order to facilitate the RNA binding to the column, immediately followed by a centrifugation at 16,000 x g for 30 seconds. 100 µL Wash Buffer (W1) were pipetted into the purification column and centrifuge for one minute at 8,000 x g as well as 100 µL Wash Buffer 2 (W2) were then added and centrifuged with the same conditions. Another wash with 100 µL of W2 Buffer was performed, followed by a centrifugation of two minutes at 16,000 x *g*.

Once the purification columns were transferred into a new 0.5 mL microcentrifuge tube, the RNA extract was collected by pipetting 13 µL of Elution Buffer directly into the filter membrane and by centrifuging firstly for one minute at 1,000 x g and then at 16,000 x g to elute RNA. The extracted RNA was stored ad -80°C before performing quality and quantitative analysis as well as Reverse Transcription Polymerase Chain Reaction (qRT-PCR).

***RNA extraction from macro-dissected HCCs and surrounding livers (FFPE samples)***

Ten micron-thick frozen sections were cut from both *Ldha* WT and *Ldha* KD tumor bearing mice. Using a scalpel, HCCs were dissected from the surrounding counterpart. The sections were collected in 0.5ml tubes and stored at -80°C until extraction. Total RNA extraction was then performed using RNeasy FFPE Kit (Qiagen, 73504). Briefly, 160 µL of Deparaffinization solution were added to dissected HCCs from both *Ldha* WT and KD mice and surrounding counterpart. Samples were then vortexed vigorously for 10s and shortly centrifuged to bring them to the bottom of the tube and incubated at 56°C for 3 min. Following the addition of 150 µL of Buffer PKD, the samples were briefly centrifuged and then added with 10 µL proteinase K. Samples were incubated at 56°C for 15 min and then at 80°C for others 15 min. The so-formed lower uncolored phase was transferred into a new 2 ml microcentrifuge tube, incubated on ice for 3 min and centrifuged for 15 min. at 20,000 x g. The supernatant was transferred into a new microcentrifuge tube. Next, 16 µL of DNase Booster Buffer equivalent were added to the samples together with 10 µL of DNase I stock solution. Samples were briefly centrifuged and incubated at room temperature for 15 min, to allow DNase to react. Afterwards, 320 µL of Buffer RBC were added to adjust binding conditions. Later on, 720 µL of 100% ethanol were added to the sample and the entire content was transferred to RNeasy MinElute spin column placed in a 2 ml collection tube before proceeding with a centrifugation of 15 s. at 8000 x g. Subsequently, 500 µL of Buffer RPE were added to the RNeasy MinElute spin column, followed by a centrifugation (15 s. at 8.000

x g). Other 500 µL of Buffer RPE were added and followed by a subsequent centrifugation (2 min. at 8000 x g). RNeasy MinElute spin column was transferred into a new 2 ml collection tube, centrifuged with open lid at full speed for 5 min., moved to a new 1.5 ml collection tube and eluted by addition of 15 µL of RNase Free Water and centrifugation for 1 min. at full speed. The extracted RNA was stored ad -80°C before performing quality and quantitative analysis as well as qRT-PCR.

***Quantitative and qualitative analysis of nucleic acids***

Total RNA concentration and purity ratio (260/280 and 260/230) were measured using Nano-Drop 1000 Spectrophotometer (Thermo-Scientific, France). RNA integrity was evaluated by Agilent Bioanalyzer 2100 (Agilent Technologies) by assessing the RNA Integrity Number (RIN). As to micro-dissected cryo-samples, only RNAs with a RIN equal to or higher than 7 were used in the study. However, all FFPE RNA samples displayed a RIN lower than 7. Nevertheless, since qRT-PCR analyses showed an almost complete similarity in the levels of gene expression changes compared to those measured in the corresponding cryo-ones, FFPE samples were also used. All procedures were performed according to manufacturer's protocol.

## Analysis of mRNA expression levels

***Reverse Transcription Polymerase Chain Reaction (RT-PCR)***

To investigate by qRT-PCR mRNA expression levels of *Glut1, Hk2, Gck, G6pd, Mct4, Glul, Glud1, Gls, Gclc, Nqo1, Ldha* and *Me1* total RNA was retro-transcribed to cDNA using the High Capacity cDNA Reverse Transcription Kit (Applied Biosystem, Life Technologies, Italy). The reaction mixture contained: 2 µL of RT buffer (10X), 2 µL of Random Primers (10X), 0.8 µL of dNTP mix (100mM), 1 µL of MultiScribe Reverse Transcriptase, 1 µL of DNase/RNase-free distilled water and 10 µL of the appropriate total RNA at the desired concentration. Thermocycler condition was: 25°C for 10 minutes, 37°C for 120 minutes and

85°C for 5 minutes, followed by a 4°C hold. Samples were then stored at -20°C until next use.

***Quantitative real-time PCR (QRT-PCR)***

Once retro-transcribed, cDNAs were used for the assessment of mRNA gene expression analysis performed by qRT-PCR. The amplification reaction was performed in a final volume of 10 µL mixture containing: 4 µL of cDNA template (2.5 ng/µl), 5 µL of 2X TaqMan Gene Expression Master Mix (Applied Biosystem, Life Technologies, Italy), 0.5 µL of 20X TaqMan assay (Applied Biosystem, Life technologies, Italy) and 0.5 µL of RNase-free water.

**Table 2. List of mouse TaqMan probes**

| Probe | Gene |
|---|---|
| Mm00441480 _m1 | Glut1/Slc2a1 |
| Mm00443385 _m1 | Hk2 |
| Mm00439129_m1 | Gck |
| Mm00656735 _g1 | G6pd |
| Mm00446102_m1 | Mct4/Slc16a3 |
| Mm00725701_s1 | Glul |
| Mm00492353_m1 | Glud1 |
| Mm00802655_m1 | Gclc |
| Mm01257297 _m1 | Gls |
| Mm001612132_g1 | Ldha |
| Mm07293397_g1 | Me1 |
| Mm01253561_m1 | Nqo1 |

## Statistical analysis

Data are expressed as mean ± standard error (SEM). Analysis of significance was done by t-Student's test and by One Way ANOVA (Tukey's post-hoc test), using the GraphPad software (La Jolla, California).

## FACS staining and Flow cytometric analysis

For flow cytometric analysis of immune cells, HCC-bearing mice were euthanized 14 weeks after hydrodynamic injection. Immediately after euthanasia, livers were collected in cold PBS and then transferred into ~ 5 ml of Digestion Buffer consisting of RPMI complete medium supplemented with 40 U/ml of Dnase I (Sigma-Aldrich D4527), 2 mg/ml of Dispase (Thermo-Fisher Scientific17105041) and 1 mg/ml of Collagenase I (Thermo-Fisher Scientific 17100-017). Tissues were then cut into small pieces using gentle MACS™ octo tissue dissociator (Miltenyi Biotec) for 15 minutes. FACS buffer (1% BSA/PBS) was added to neutralize the reaction. To obtain single cells suspension, the homogenate was filtered with a 70 μM cell strainer, incubated with red blood Cell Lysis buffer (Sigma-Aldrich R7757), and filtered again with 40 μM cell strainer. Single cells were resuspended in FACS buffer (1% BSA/PBS) and blocked for 15 min with anti-CD16/CD32 (Mouse FC block, 553142 BD Biosciences) at 4°C. To detect cell surface antigens, samples were stained for 30 min at 4°C with fluorochrome-conjugated antibodies and washed prior to the analysis. For intracellular antigen staining, samples stained for the extracellular antigens, as described above, were then washed with FACS buffer, centrifuged and resuspended in 100 μL of 1X Fixation/Permeabilization working solution - 1 part of Fixation/Permeabilization Concentrate (Invitrogen 00-5123-43) with 3 parts Fixation/Permeabilization Diluent (Invitrogen 00-5223-56) - for 30 min. at 4°C. Subsequently, 150 μL of 1X Permeabilization Buffer (Invitrogen 00-8333-56) were added. Finally, cells were washed, centrifuged and resuspended in 200 μL of FACS buffer or, alternatively, in a mix of 100 μL of FACS buffer and 100 μL of IC fixation buffer (Invitrogen 00-8222-49) prior to analysis. After beads compensation with UltraComp eBeads™

Compensation Beads (Invitrogen 01-2222-42) in order to set voltages and gating parameters for obtaining accurate fluorescence signal, data were collected with both FACS Canto (BD Biosciences) and FACS Verse (BD Biosciences).

**Table 3: List of primary antibodies**

| Antibody | Dilution |
|---|---|
| Fixable Viability Dye eFluor™ 506 (Invitrogen 65-0866-14) | 1:500 |
| APC/Cyanine7 anti-mouse CD45 (Bio Legend 103116) | 1:300 |
| PerCP/Cy5.5 anti-mouse F4/80 [BM8] (BioLegend 123128) | 1:100 |
| BV421 anti-mouse CD335 (NKp46) [29A1.4] (BioLegend 137612) | 1:100 |
| PE Rat Anti-Mouse Ly-6G (BD Pharmingen 551461) | 1:500 |
| MHC Class II (I-A/I-E) Monoclonal Antibody (M5/114.15.2), FITC (Invitrogen 11-5321-82) | 1:400 |
| CD206 AlexaFluor647 [MR5D3] rat IgG2a (Biorad MCA2235A647T) | 1:100 |
| Anti-Mouse CD11b eFluor 450 [M1/70] Rat (eBioscience 48-0112-82) | 1:200 |
| Anti-Mouse CD8a Alexa Fluor 488 [53-6.7] Rat (eBioscience 53-0081-82) | 1:300 |
| PE anti-mouse CD279 (PD-1) [29F.1A12] (BioLegend 135206) | 1:200 |
| PerCP/Cy5.5 anti-mouse CD4 [RM4-5] (BioLegend 100540) | 1: 200 |
| Anti-Mouse CD25 PE-Cy7 (PC61.5) (eBioscience 25-0251-82) | 1:200 |
| Anti-Mouse/Rat Foxp3 APC (FJK-1612) (eBioscience 17-5773-82) | 1:100 |

# RESULTS

## C-Myc-h-Ras tumors metabolism characterization

We utilized a very aggressive carcinogenesis model whereby HCC was induced by overexpression of Harvey rat sarcoma viral oncogene homolog (h-Ras$^{G12V}$) and c-MYC oncogenes. We employed a liver-specific promoter to specifically express the oncogenes in cells of the hepatic lineage. Since HCC usually develops in adults via somatic mutations, the oncogene expression during early embryonic development might lead to embryonic lethality or unexpected abnormal characteristics, increasing the discrepancy between the HCC animal model and human HCC (78). To avoid this possibility, we induced stable oncogene expression into young adult mice (6 to 8 weeks old mice).

PiggyBac (PB) transposons were designed to express h-Ras$^{G12V}$ and c-Myc under the control of the hepatocyte-specific transthyretin minimal (TTRmin) promoter (79). In order to develop the most reliable and effective model, we tested different concentration of oncogenes combination in experimental trials, after which we selected the concentration of 0.1 μg for the future experiments.

Therefore, studies were performed in mice hydrodynamically co-transfected with 0.1 μg of transposon plasmids expressing h-Ras$^{G12V}$, c-Myc (PB-h-Ras$^{G12V}$ and PB-c-Myc) and hyperactive PB to ensure efficient transgene integration.

As shown in **Fig. 1A**, combination of the two oncogenes led to HCC development in 100% of mice at 14 weeks after transfection. These results show a rapid occurrence of HCCs as the result of the cooperative action of the h-Ras$^{G12V}$ and c-Myc oncogenes (79).

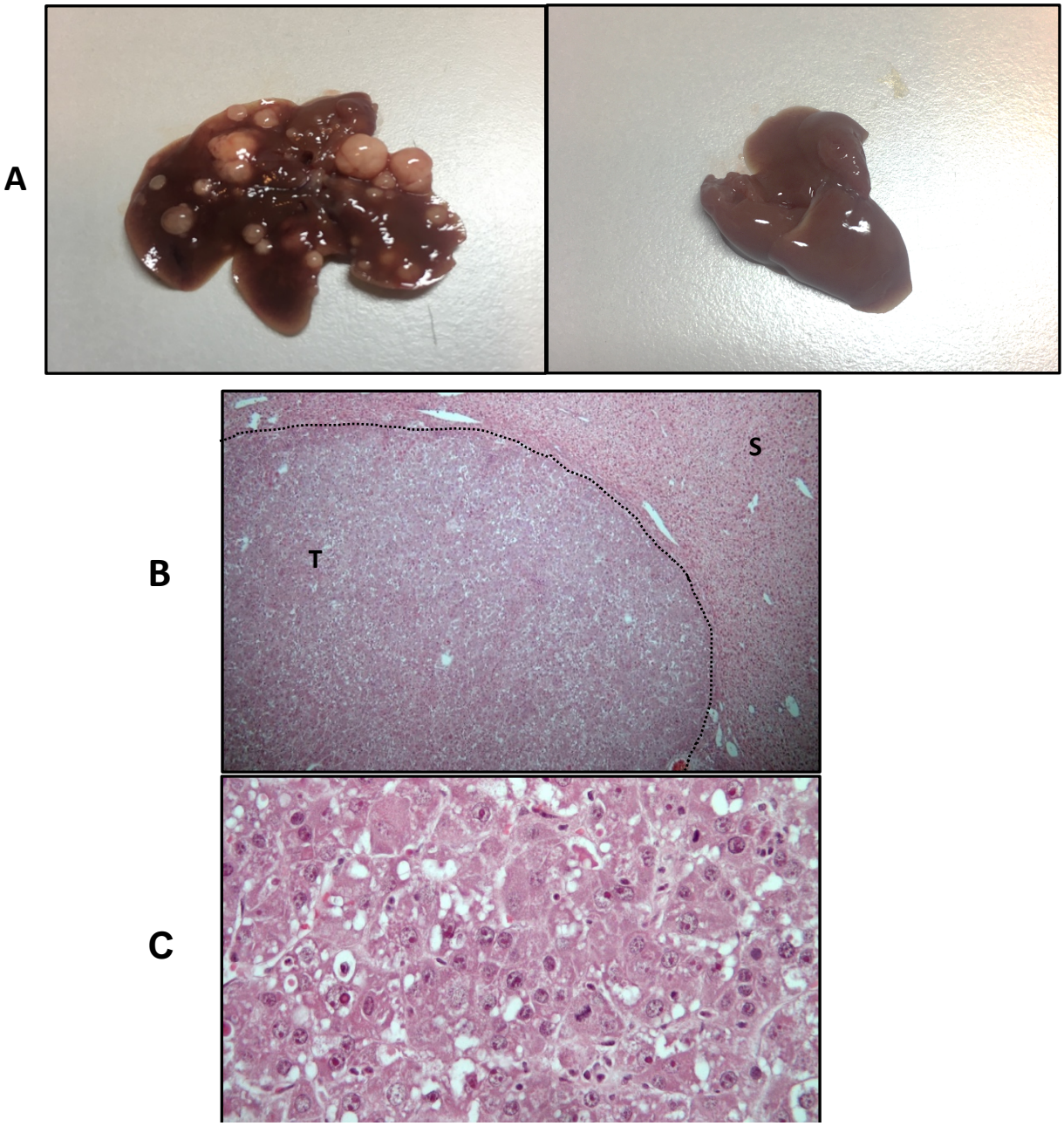


**Figure 10. A) Left: Macroscopic view of the liver from C-MYC-HRAS mice 14 weeks after hydrodynamic injection; Right: Liver from mice subjected to hydrodynamic injection without oncogene-carrying plasmids; B) Microscopic examination of C-MYC-HRAS tumor model (H&E. Magnification 5x) C) Microscopic examination of C-MYC-HRAS tumor model 40x (H&E. Magnification 40x).**

The c-Myc-h-Ras oncogene combination led to the formation of multifocal widely distributed HCCs of variable size, which appeared paler compared to the non-tumoral area. Microscopic analysis revealed well-differentiated trabecular HCCs that spread extensively within the liver both by invasion and compression of surrounding area. Tumoral lesions displayed an intense basophilic cytoplasm, and a strong nuclear atypia characterized by the presence of several nucleoli. Apoptotic bodies and mitoses were also observed. Frequently, the tumor

edge was invaded by inflammatory cells, with features resembling a pseudo-follicular organization. On the other hand, the structural architecture of surrounding area appeared to be well-conserved. (**Fig. 10B,10C**)

As expected, all HCCs displayed a strong nuclear staining of c-Myc **(Fig. 11A**) and were characterized by a very high proliferative activity as demonstrated by a uniform staining with Ki-67 **(Fig. 11B)**, a nuclear protein associated with cellular proliferation and a prognostic parameter in many human tumors, including HCC (80).

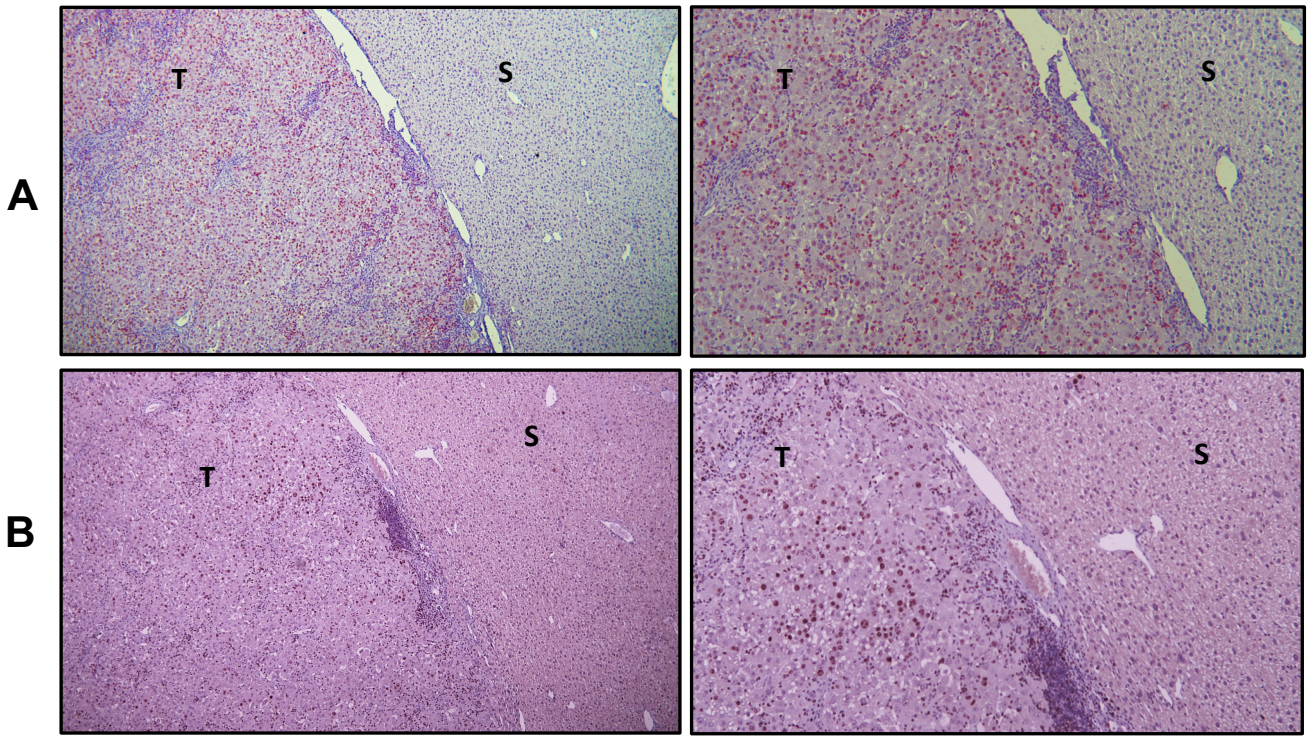


**Figure 11. A) Mouse liver sections showing nuclear red staining of C-Myc in the cancer cell nuclei (HCC) but not in surrounding (S) liver (Left: Magnification 5x – Right: Magnification 10x). B) Serial sections showing Ki-67 positive brown nuclear staining in tumors (Left 5x - Right 10x).**

It has been reported that c-Myc-driven liver tumors display increased glucose uptake and support its catabolism into lactate with the concomitant upregulation of pivotal glycolytic enzymes. Moreover, c-Myc promotes glutaminolysis in order to fuel the TCA cycle (72). (**Fig. 12).**

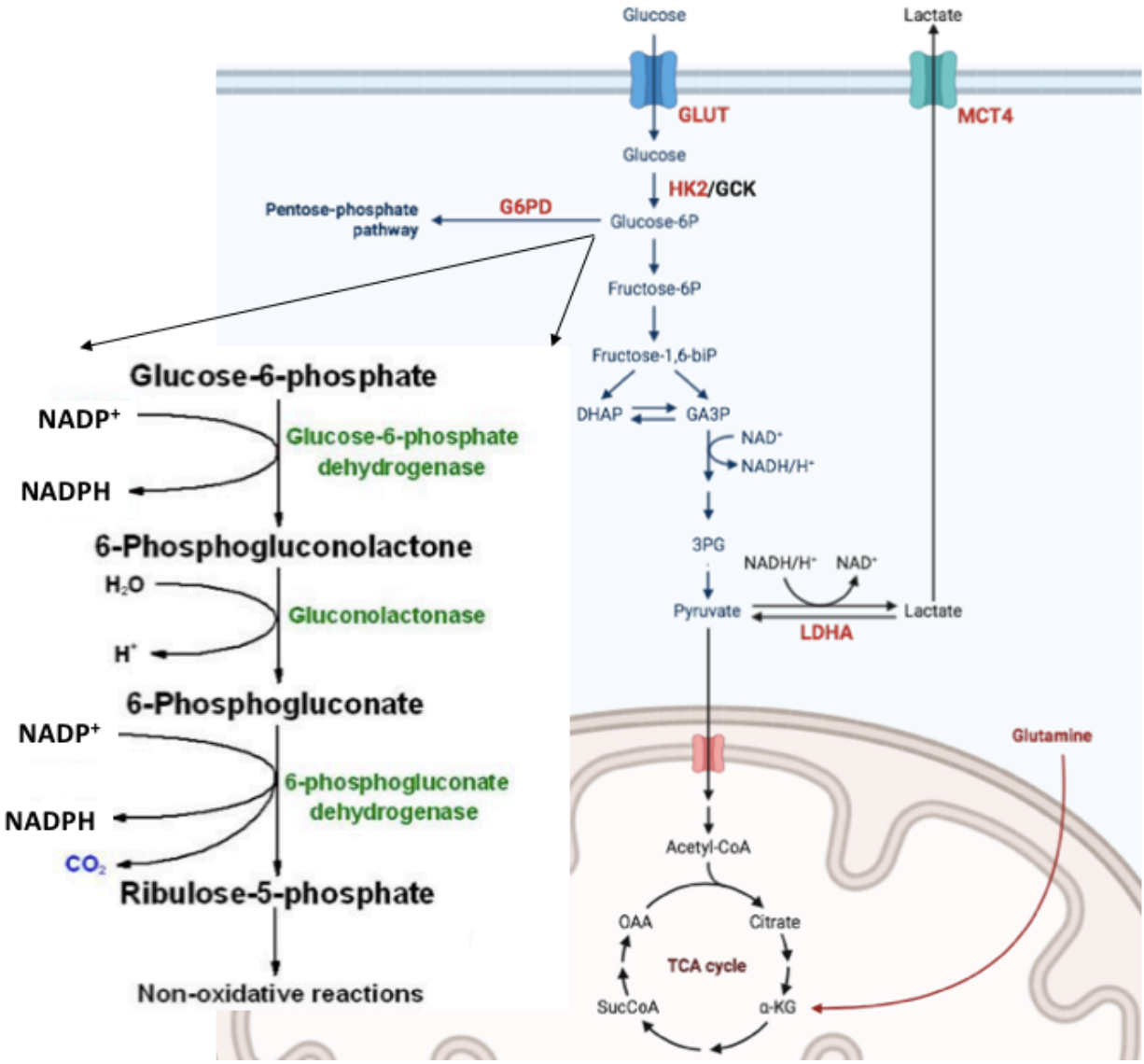


**Figure 12. Schematic representation of altered biochemical pathways in C-MYC-HRas-induced HCC. Red color indicates increased expression/activity**

However, metabolic alterations in the c-Myc/h-Ras model have never been described. Since many metabolic changes have been shown to be strictly oncogene-dependent, we aimed at characterizing the metabolic profile of HCCs developed by the c-Myc/h-Ras experimental model.

HCCs have been shown to undergo metabolic reprogramming and exhibit a strong glycolysis dysregulation (23,53,55,56). Accordingly, qRT-PCR analysis performed on laser-micro-dissected tumors or peritumoral tissues, revealed that the glucose transporter 1 (*Glut1*) was upregulated in tumor cells, compared with the surrounding tissue, suggesting

an increased glucose uptake by cancer cells (**Fig. 13**). Consequently, Hexokinase 2 (*Hk2*) - a tumor-specific kinase and the isoform of the first enzyme of glycolysis Glucokinase (*Gck*) - was strongly increased in the tumor compared with the surrounding tissue **(Fig. 13**).

The final step of glycolysis is the conversion of pyruvate to lactate catalized by lactate dehydrogenase A (LDHA) and its extrusion from the cell to the extracellular matrix, through the monocarboxylate transporter Mct4. In agreement with the increased glucose uptake, Ldha activity and *Mct4* expression were significantly enhanced in tumoral tissue compared to the surrounding liver (**Fig. 13)**.

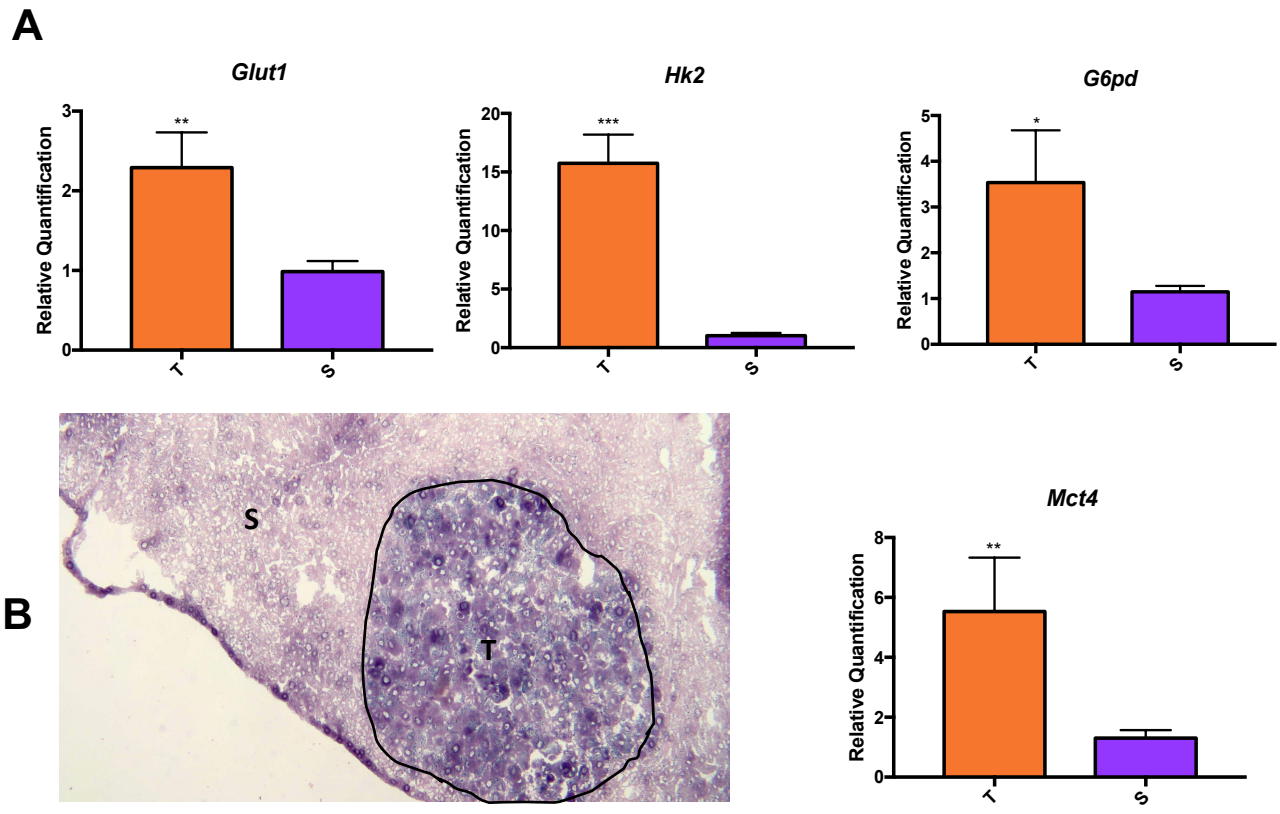


**Figure 13. A) qPCR analysis of *Glut1, Hk2, G6pd* in tumors compared to surrounding area from both FFPE and frozen samples; B) Ldha activity in tumors (T) and surrounding area (S) and qPCR analysis of *Mct4.* qRT-PCR analysis was performed on dissected tumors or surrounding livers. Gene expression is reported as fold-change of tumor mRNA relative to surrounding livers. The histogram represents mean values + SD of 6 Tumors and 4 surrounding liver sections. (*t*-test) *P<0.05; **P<0.01*** P<0.001.**

It has been shown that, as a consequence of the metabolic reprogramming occurring in tumors, glycolytic intermediates are redirected towards the PPP (81). Indeed, *G6pd*, the

rate-limiting enzyme of the oxidative branch of the PPP is upregulated in order to cope with the increased demand for riboses - required for the synthesis of many biological building blocks, such as nucleic and fatty acids to sustain cell proliferation - and the need of reducing equivalent nicotinamide adenine dinucleotide phosphate (NADPH), to counteract the increased generation of reactive oxygen species (ROS) and enhance tumor cell survival. Accordingly, IHC analysis showed that the expression of G6pd was strongly induced in tumors while being virtually negative in the peritumoral area. (**Fig. 14**)

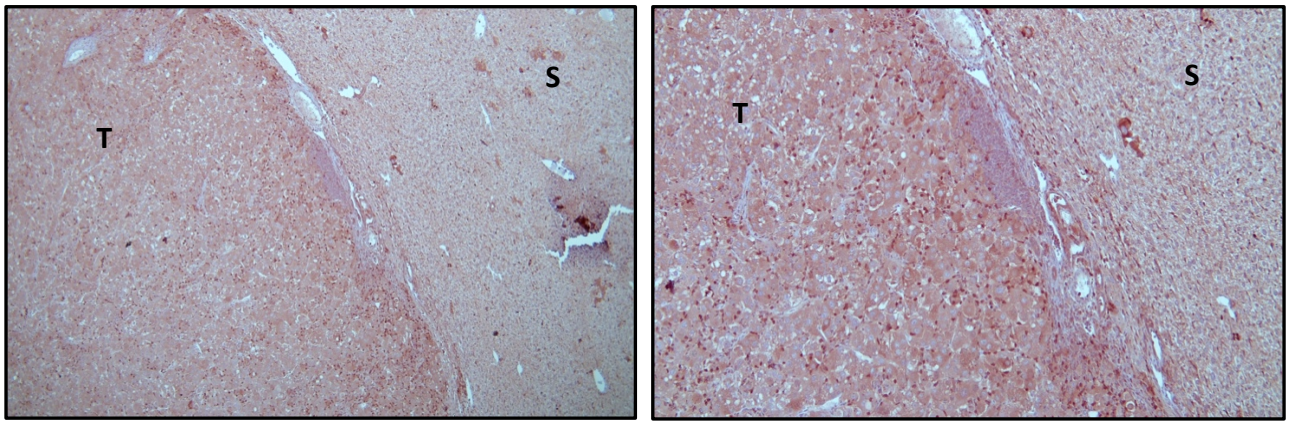


**Figure 14. Microphotographs showing G6pd immunostaining in HCC compared to peritumoral areas (G6pd staining: 5x (Left); 10x (Right)**

Together with increased glucose uptake, tumor cells are often characterized by changes in glutamine metabolism. Notably, c-Myc has been shown to promote glutaminolysis in order to fuel TCA cycle (72). Therefore, we wished to determine the fate of glutamine in the tumors generated by the c-Myc/h-Ras model. Immune-staining of Glutamine synthase (Gs), the enzyme that catalyzes the conversion of glutamate into glutamine, revealed that while this enzyme was present in the hepatocytes surrounding the terminal hepatic venules, it was completely absent within the tumors (**Fig. 15**)

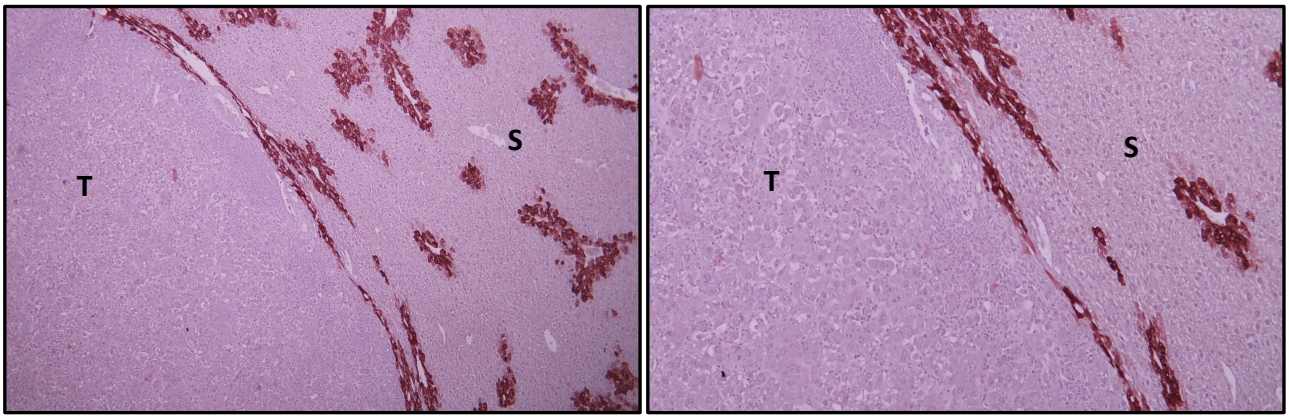


**Figure 15. Immunohistochemistry illustrating a complete absence of Gs in HCC. Surrounding liver (S) shows an intense staining of the hepatocytes encompassing the hepatic terminal venules (Gs: 5x (Left) – 10x (Right 10x).**

Further analysis showed that the lack of Gs protein was the consequence of down-regulation of transcription of *Glul,* the gene coding for Gs. Indeed, qRT-PCR analysis revealed that *Glul* mRNA levels in tumoral hepatocytes were significantly reduced compared to the surrounding tissue, indicating an almost complete inhibition of *Glul* transcription in cancer cells (**Fig. 16)**.

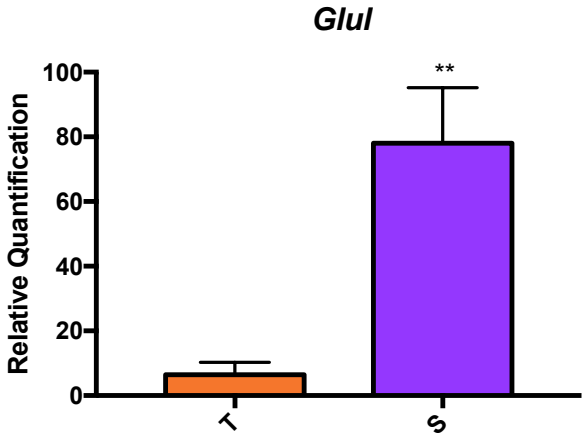


**Figure 16. qPCR analysis of *Glul* mRNA levels in tumors compared to surrounding area. qRT-PCR analysis was performed on dissected tumors (T) or surrounding livers (S). Gene expression is reported as fold-change of tumor mRNA relative to surrounding livers. The histogram represents mean values + SD of 6 Tumors and 4 surrounding liver sections. (*t*-test) **P<0.01.**

Gs is a direct target of activated β-Catenin which is frequently mutated/overexpressed in human and rodent HCCs (82–84). To understand whether the lack of Gs observed in the tumors could be due to down-regulation of β-catenin, we performed IHC. The results showed

that all tumors displayed a strong β-catenin accumulation in spite of the lack of Gs expression, ruling out the possibility that its loss could be the consequence of down-regulation of β-catenin (**Fig. 17A**).

On the other hand, glutaminolysis was strongly increased in tumors compared to surrounding liver, as shown by the intense immune-staining for glutaminase (Gls), the enzyme responsible for the conversion of glutamine into glutamate, unveiling that the combination of c-Myc-h-Ras oncogenes promotes glutamine catabolism (**Fig. 17B**).

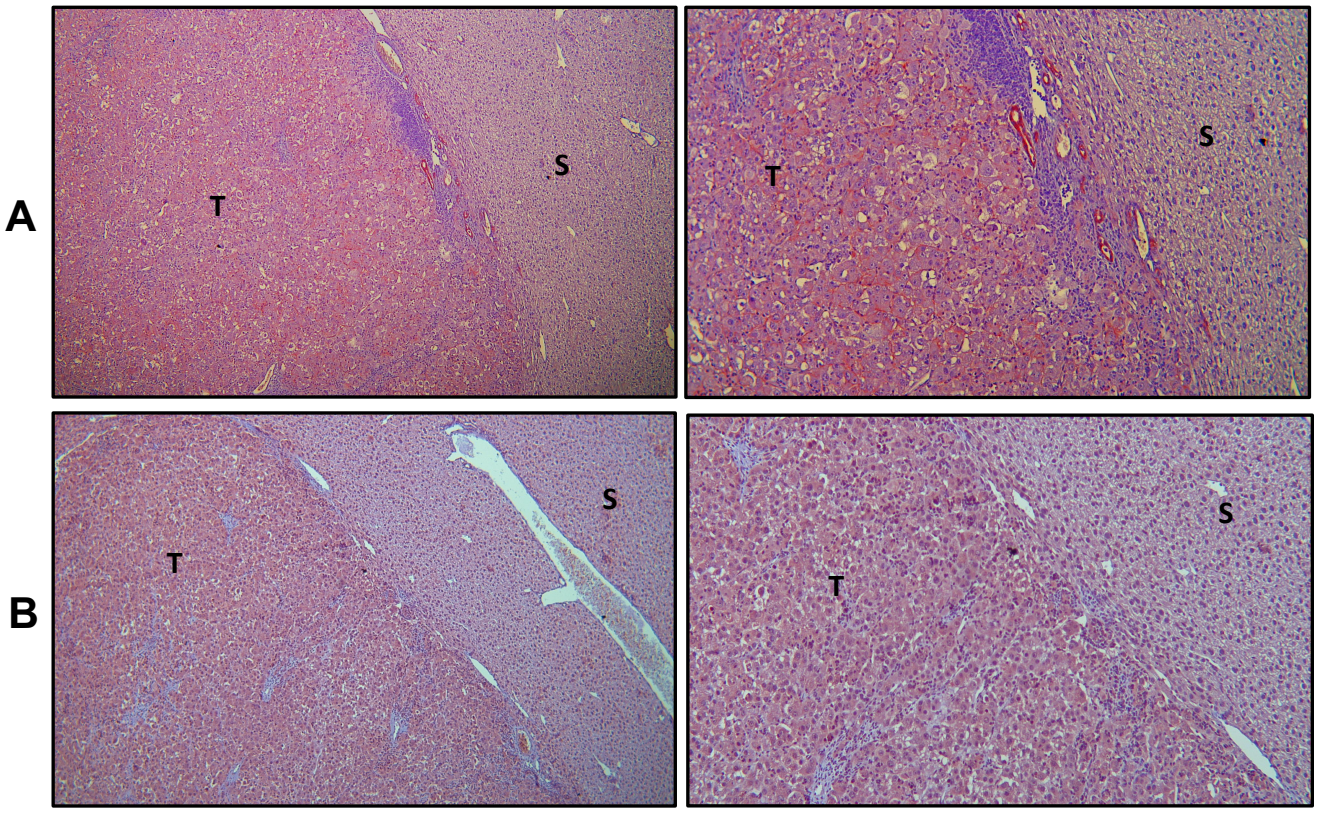


**Figure 17. A) IHC of β-catenin, and B) Gls positive tumors (T) compared to peritumoral area (S). (Left 5x - Right 10x).**

Based on the finding of the impairment of glutamine synthesis and increased glutamate content due to glutaminolysis, we next wished to assess the fate of the increased glutamate accumulation. As shown in **Fig. 18**, glutamate undergoes two possible fates: on the one hand, glutamate can be redirected into the TCA cycle after its conversion in α-ketoglutarate;

on the other hand, it can be utilized to the synthesis of glutathione which is needed to counteract cellular injury caused by oxidative damages.

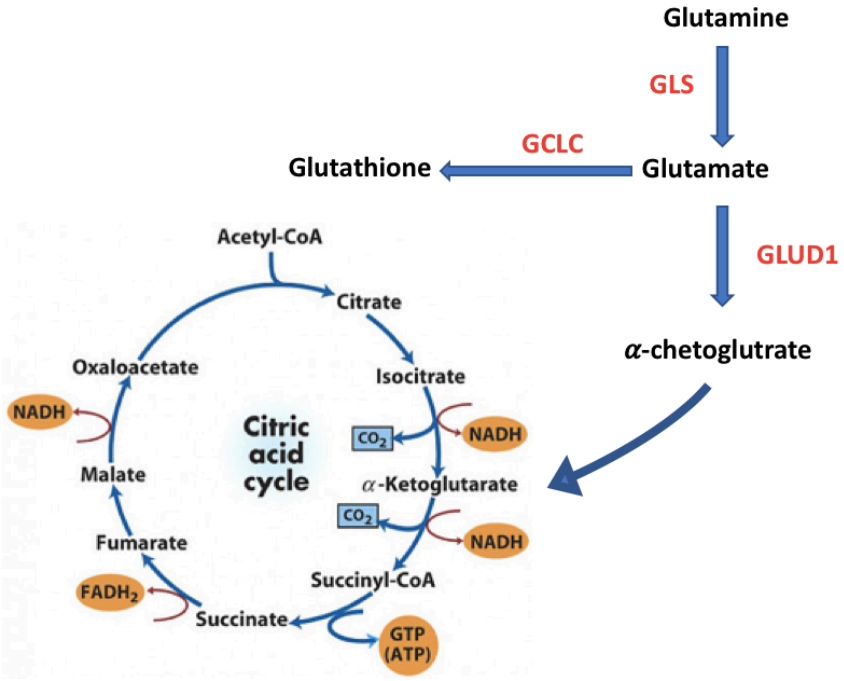


**Figure 18. Representative scheme illustrating two alternative fates of glutamine.**

Therefore we analyzed the expression of *Glud1*, the enzyme responsible for the conversion of Glutamate into α-ketoglutarate, and of *Gclc* which is involved in the conversion of Glutamate into Glutathione. (**Fig. 19**).

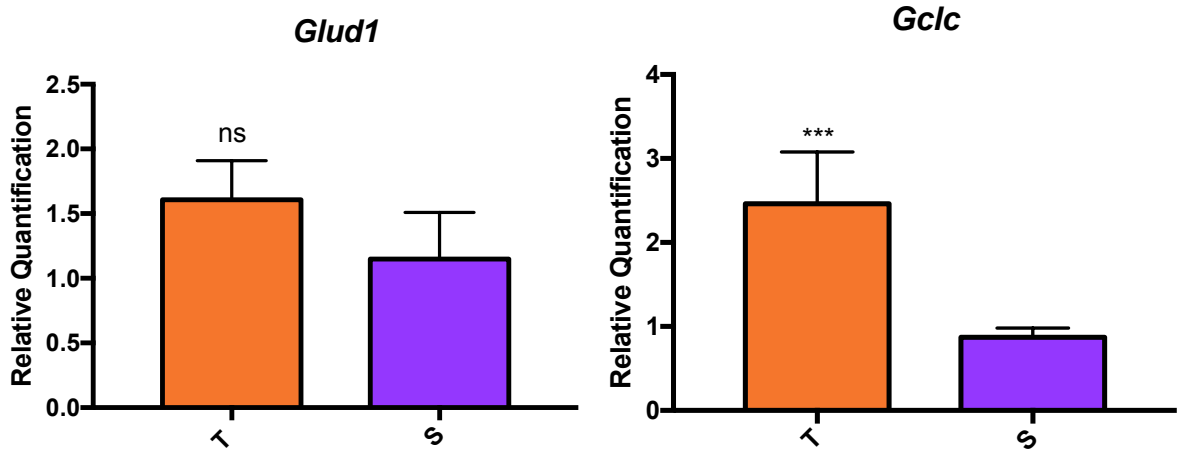


**Figure 19. qPCR analysis of *Gclc and Glud1* mRNA levels in tumors compared to surrounding area. qRT-PCR analysis was performed on dissected tumors (T) or surrounding livers (S). Gene expression is reported as fold-change of tumor mRNA relative to surrounding livers. The histogram represents mean values + SD of 6 Tumors and 4 surrounding liver sections. (*t*-test ). ns: not significant; ***P<0.001.**

As reported in **Fig. 19**, no significant change in *Glud1* mRNA levels between tumors and surrounding liver was observed, suggesting that the excess of catabolized glutamine is not utilized as a fuel for the TCA cycle. Conversely, the expression of *Gclc*, the enzyme involved in glutathione synthesis, was strongly increased in tumor cells compared to the peritumoral tissue. These findings further support that the increased glutaminolysis is not used to sustain TCA cycle but rather to convert glutamate into glutathione in order to protect cancer cells from oxidative damage usually occurring in rapidly growing tumors.

Although an increased glycolysis in HCC has been often associated with a decreased OXPHOS (56,85), our understanding of the modifications of TCA and OXPHOS occurring in HCC and in MYC driven tumors, remains controversial (56,86–88). Hence, we measured the activity of succinate dehydrogenase A (Sdha) - the major catalytic subunit of succinate-ubiquinone oxidoreductase - that converts succinate into fumarate. Importantly, Sdha is part not only of the TCA cycle, but it is also a complex of the mitochondrial respiratory chain, specifically complex II (89,90). Histochemical analysis performed on cryostat sections showed that the activity of Sdha was severely impaired in c-Myc/h-Ras tumors compared to the peritumoral area (**Fig. 20**).

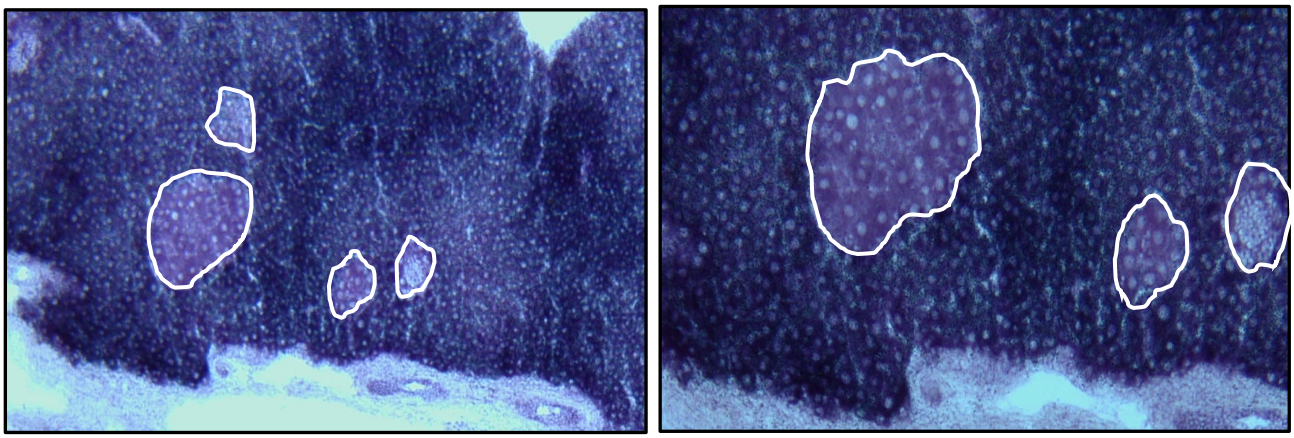

**Figure 20) Histochemistry of Sdha showing a remarkable decrease of enzyme activity in c-Myc-h-Ras tumors (outlined areas) compared to the surrounding tissue (Left 5x, Right 10x).**

Taken together, these results demonstrate that c-Myc/h-Ras oncogene model leads to a metabolic reprogramming characterized by increased glucose uptake and lactate production, enhanced PPP and impairment of OXPHOS. Among the genes found up-regulated in HCCs were *G6pd* and *Gclc*. Interestingly, these genes are target of the transcription factor Nuclear factor erythroid 2-related factor 2 (Nrf2), which promotes transcription of a number of genes involved in cellular protection **(Fig.21)**(91,92). Notably, Nrf2 has been shown to be an important actor in metabolic reprogramming by redirecting glucose and glutamine into anabolic pathways (56,81). Therefore, we wondered whether the metabolic reprogramming observed in our c-Myc/h-Ras tumor model could be a consequence of activation of the Nrf2-Keap1 pathway.

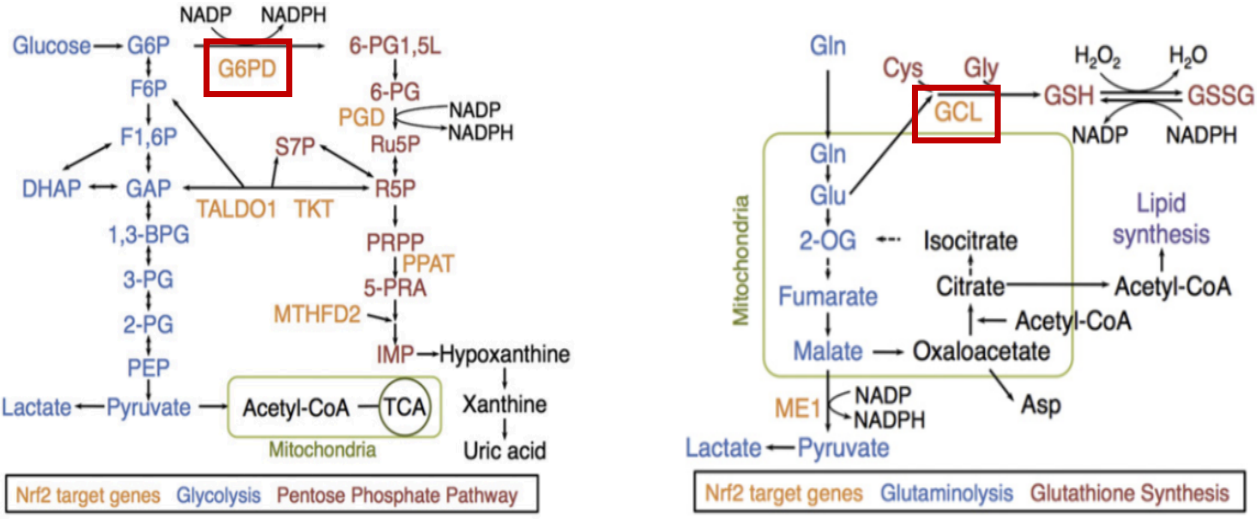


**Figure 21 Schematic representation of Nrf2 pathway target genes. Slightly modified by Mitsuishi et al.(81).**

To address this question, we determined the expression of NAD(P)H dehydrogenase quinone 1 (*Nqo1*), the best characterized Nrf2-target gene. As shown in **Fig. 22** no significant differences in the expression of *Nqo1* mRNA was observed between tumors and peritumoral area, suggesting that NRF2-KEAP1 pathway was not involved in the metabolic reprogramming observed in HCC.

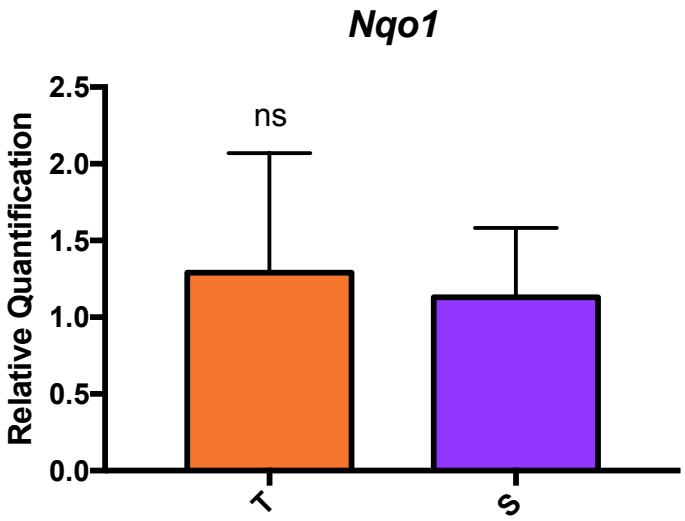


**Figure 22. qPCR analysis of *Nqo1* mRNA levels in tumors compared to surrounding area. qRT-PCR analysis was performed on dissected tumors (T) or surrounding livers (S). Gene expression is reported as fold-change of tumor mRNA relative to surrounding livers. The histogram represents mean values + SD of 5 Tumors and 4 surrounding liver sections. (*t*-test). ns: not significant.**

## Effect of *Ldha* KD on tumor growth

One of the consequences of increased glycolysis at the expense of OXPHOS is an increased lactate production which is extruded through the transporter Mct4 to the extracellular space causing injury-induced acidification of the surrounding environment and, therefore increasing the invasive capacity of tumor cells (93,94). Therefore, having characterized the c-Myc/h-Ras model, we wished to investigate whether knocking down (KD) of *Ldha* could lead to an impairment of the metabolic reprogramming observed in c-Myc/h-Ras HCC. Along these lines, we assessed how *Ldha* loss could affect the expression level of the pivotal enzymes involved in the observed metabolic reprogramming.

In order to examine the effect of *Ldha* loss on the growth of hepatic tumors, we knocked down *Ldha* exclusively in transformed hepatocytes to achieve a more accurate genetic functional study. We used the tamoxifen-regulated Cre-loxP system, in which temporal expression of a gene of interest, in a specific cell type can be induced by treatment with tamoxifen. In our model, tamoxifen-activated Cre leads to selective *Ldha* deletion in hepatocytes.

Conditional *Ldha* lox/lox mice subjected to hydrodynamic injection of c-Myc and h-Ras expressing plasmids, together with Cre, were splitted after 4 days into two groups: the first group was left untreated while the second group was injected with Tamoxifen for 5 consecutive days (1mg/mouse/day). Animals were killed 14 weeks after the hydrodynamic injection.

As shown in **Fig. 23** the hepatocyte-specific *Ldha* knock-down led to a strong tumor reduction in terms of both number and size.

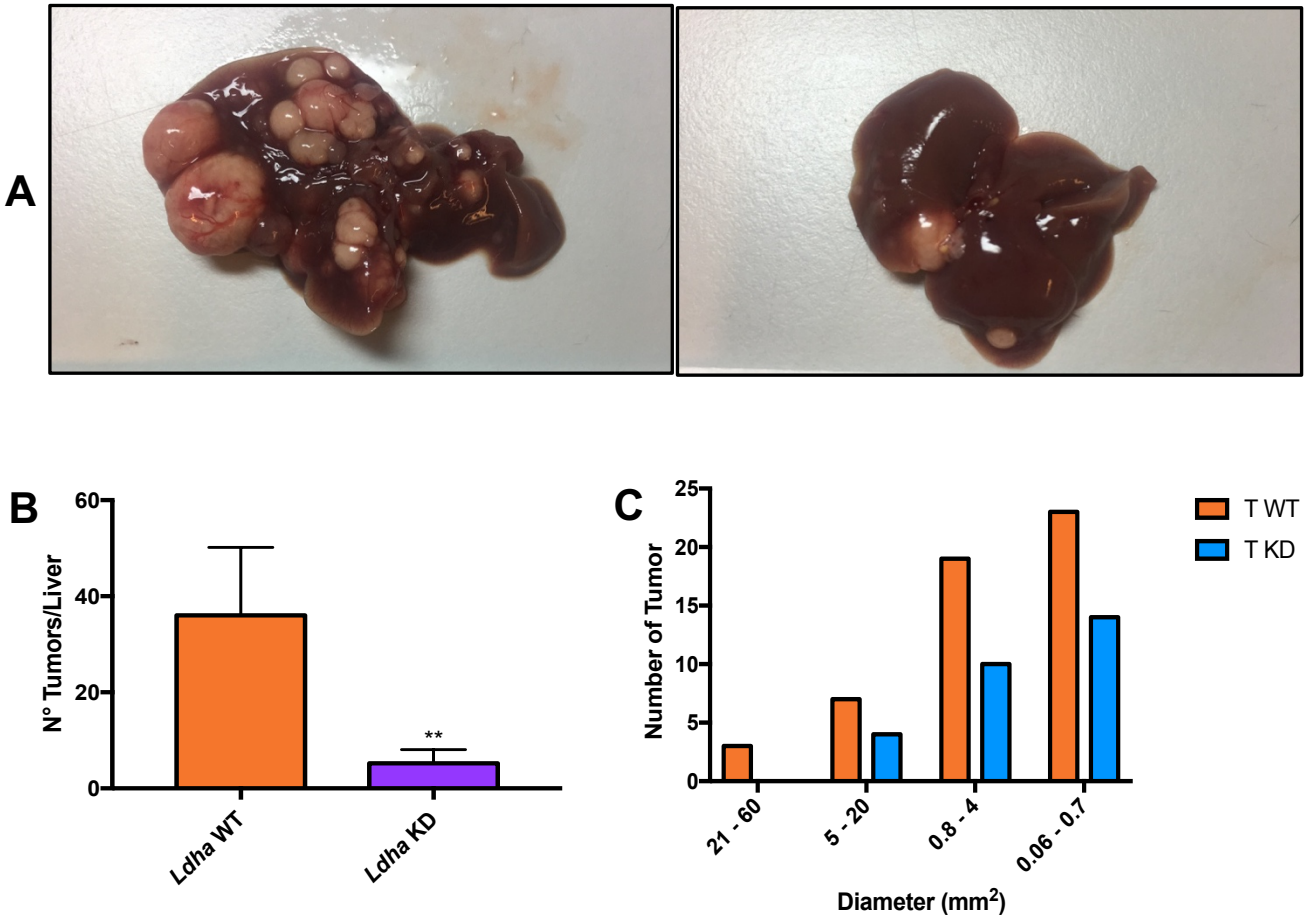


**Figure 23. A) Macroscopic view of livers from *Ldha* WT or KD mice. B) Number of tumors in *Ldha* WT and KD mice; C) Average of the size of *Ldha* WT or KD tumors. (*t*-test). **P < 0.01. Number and tumor size were evaluated in H&E stained histological sections.**

Using the same laser-microdissection technology previously described, we extracted mRNA from tumors or surrounding liver of WT and KO mice. To validate our KO procedure we evaluated the levels of *Ldha* transcripts in WT and KO tumors. However, the expression of *Ldha* in KO tumors revealed that it was significantly lower (~70%) than that observed in

WT HCCs but not completely abrogated, thus providing an efficient knock- down (KD) model (**Fig. 24).**

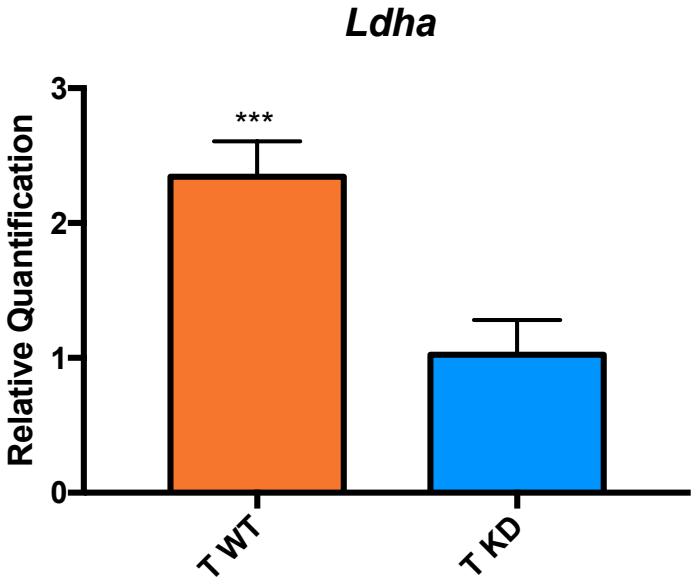


**Figure 24. qPCR analysis of *Ldha* mRNA levels in laser-microdissected WT HCCs compared to *Ldha* KD tumors. Gene expression is reported as fold-change of mRNA from WT tumors relative to those from *Ldha* KD livers. The histogram represents mean values + SD of 6 to 4 tumors/group. (*t*-test). ***p < 0.001.**

To understand the cause of the reduced number and size of *Ldha* KD HCCs, we investigated whether it could be the consequence of 1) a reduced proliferation rate or, 2) an increased death of cancer cells by apoptosis.

To address the first question, we performed immunostaining of Ki-67 in both *Ldha* WT and KD tumors. As shown in **Fig. 25**, a striking proliferative activity was detected in both the groups. Indeed, tumors showed a very high proliferation activity compared to the peritumoral area in either group. Therefore, we can conclude that the tumor reduction observed in *Ldha* KD is not a consequence of a lower tumor cell proliferation in KD mice.

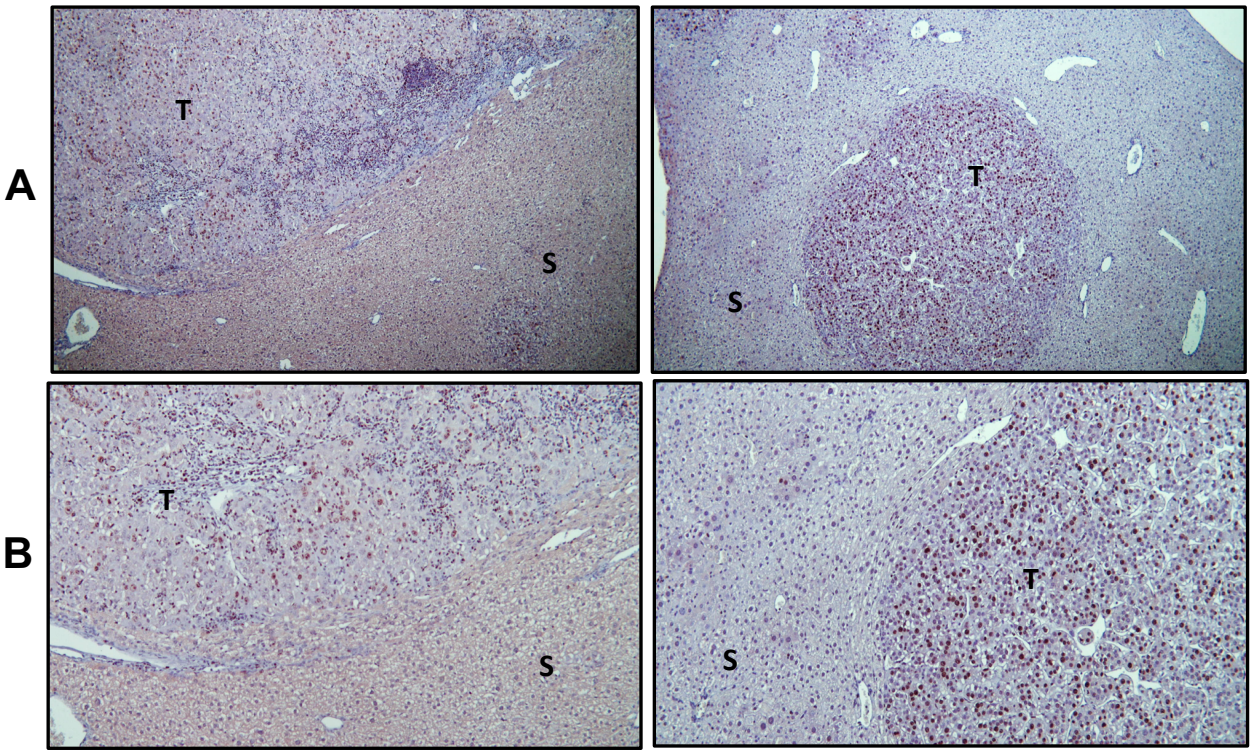


**Figure 25. Representative microphotographs of immunohistochemical staining for Ki-67 in the tumors (T) or surrounding livers (S) of *Ldha* WT (A) or *Ldha* KD mice (B). (Left X5; Right X10; sections counterstained with hematoxylin)**

Next, we investigated whether an increased apoptotic rate in *Ldha* KD tumors could account for the reduced tumor size. However, immunohistochemical staining for the cleaved form of Caspase 3 (Casp3) showed that while the apoptotic index in both WT and *Ldha* KD tumors was much higher than their corresponding peritumoral tissues, it was not significantly different between the two groups (**Fig. 26**). Thus, apoptosis cannot explain the reduction of tumor number and size observed in *Ldha* KD mice.

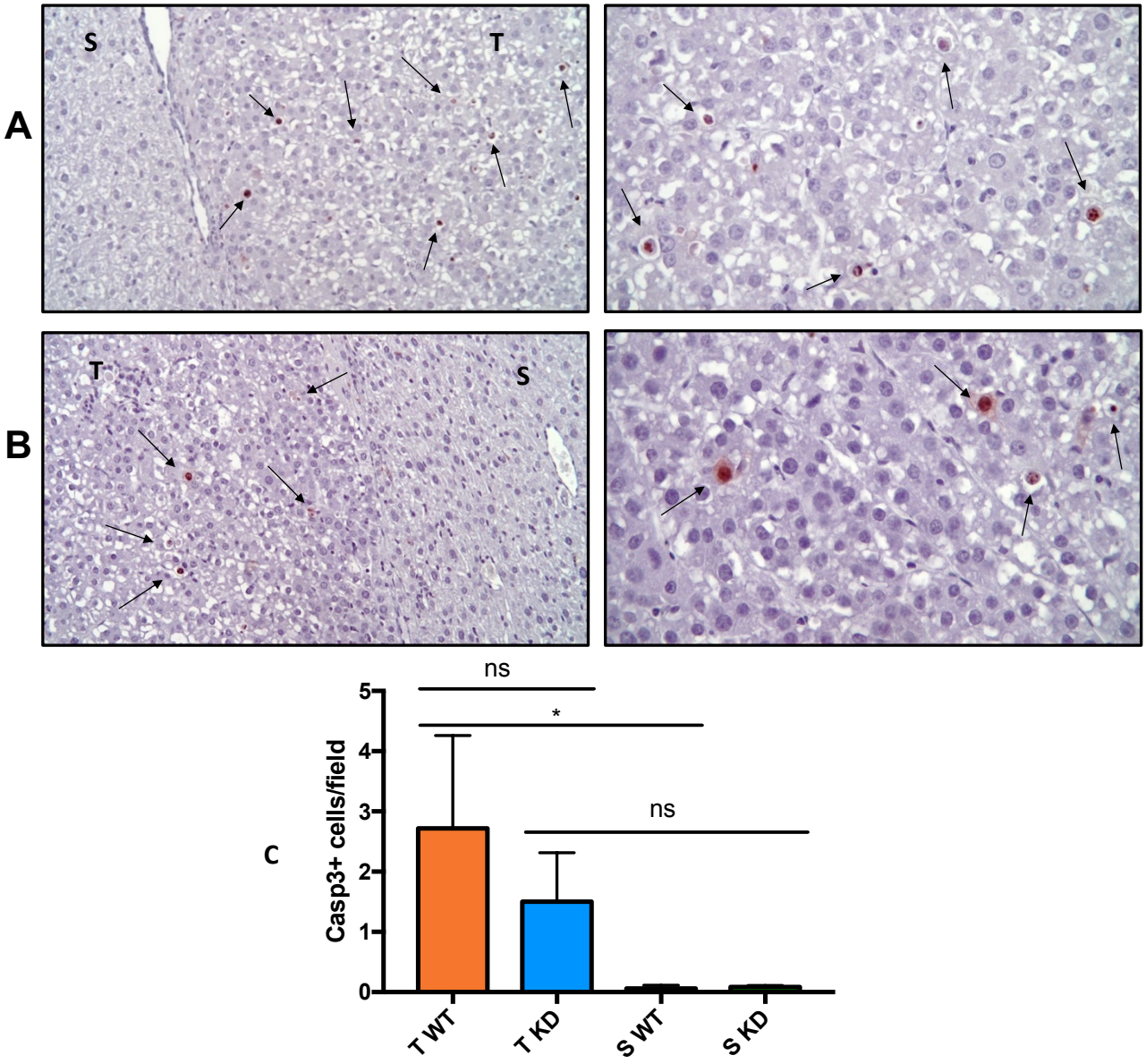


**Figure 26. Representative microphotographs showing immunostaining for the cleaved form of caspase-3 (Casp3) in the tumors (T) or surrounding liver (S) of *Ldha* WT (A) and KD (B) mice. (Casp3 counterstained with Hematoxylin, X20, left; X40 right). Arrows indicate single Casp3 positive cells; C) Apoptotic index (AI). AI was calculated as the number of Casp3 positive cells/per field at X40 magnification. From 20 to 40 fields per liver were scored. Results were expressed as means ± S.E. of 3-4 mice per group. (one way ANOVA).**

As previously shown, metabolic reprogramming consisting of a switch from OXPHOS to glycolysis characterizes the c-Myc-h-Ras model. Therefore, we considered the hypothesis that metabolic reprogramming was somehow impaired in *Ldha* KD tumors, thus

limiting tumor growth and progression. To investigate whether *Ldha* loss could impact on the overall metabolic reprogramming, we examined by qRT-PCR and IHC the expression of several components implicated in glycolysis, PPP and OXPHOS. As shown in **Fig. 27** the expression of *Glut1* was significantly downregulated in KD tumors compared to WT ones, and was not different from that observed in the surrounding liver highlighting a lesser glucose uptake by cancer cells in the absence of *Ldha*. Notably *Ldha* KD HCC also displayed decreased expression, albeit not significant, of the pro-tumoral isoform *Hk2* and an enhanced expression of *Gck* compared WT HCC.

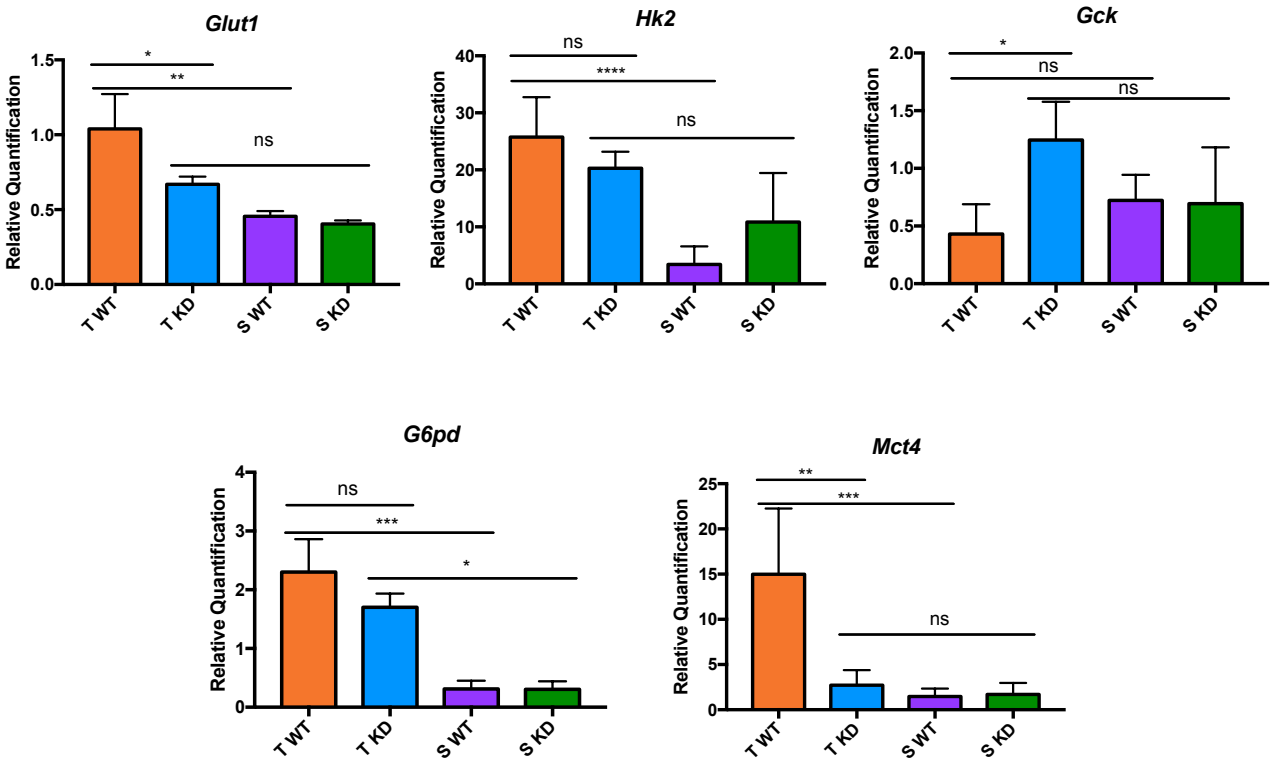


**Figure 27. qRT-PCR analysis of the expression of *Glut1, Hk2, Gck, G6pd and Mct4*. Relative quantification analysis for each gene was calculated by $2^{-\Delta\Delta Ct}$ method. (one way ANOVA). ns: not significant. **P*<0.05; ***P*<0.01; ****P*<0.001.**

Next, we examined activation of the PPP by measuring the expression of the rate limiting enzyme G6pd. Accordingly to IHC, the expression of G6pd was significantly enhanced in KD HCC compared to surrounding liver (**Fig. 28**). The levels of *G6pd* mRNA

were also elevated compared to peritumoral liver, although slightly lower than those observed in WT animals (**Fig. 27**). These findings indicate that loss of *Ldha* only minimally affects PPP activation.

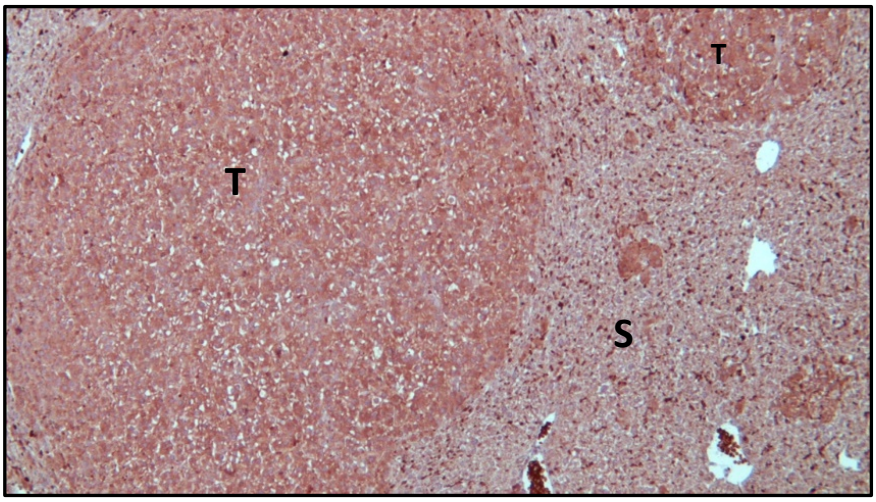


**Figure 28. Microphotographs showing G6pd immunostaining in *Ldha* KD tumors (T) compared to peritumoral areas (S) (10x magnification).**

Conversely, while the expression of the lactate transporter *Mct4* was strongly up-regulated in WT HCCs, no change in *Mct4* mRNA levels was observed between *Ldha* KD tumors and the surrounding liver. The expression of *Mct4* in *Ldha* tumors was found strongly down-regulated when compared to WT HCCs (**Fig. 27**).

As previously shown (**Fig. 19**), while no significant change occurred in *Glud1* mRNA levels occurred between tumors and surrounding liver of wild type mice, the expression of *Gclc*, the enzyme involved in the synthesis of glutathione, was enhanced in tumor cells compared to the peritumoral tissue. These results support the hypothesis that the increased glutaminolysis is not used to sustain TCA cycle but rather to convert glutamate into glutathione in order to protect cancer cells from oxidative damage usually occurring in rapidly growing tumors (**Fig. 29**).

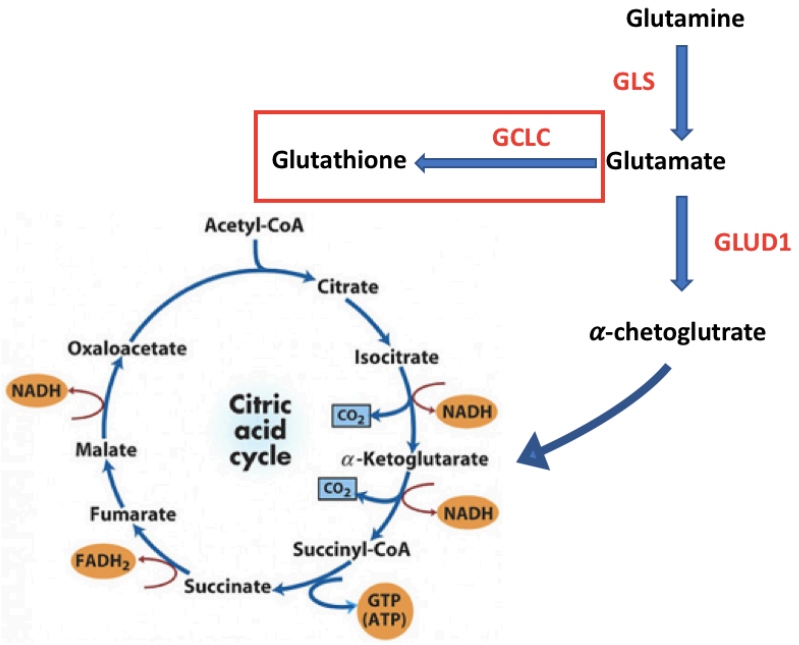


**Figure 29. Schematic representation illustrating the preferential conversion of glutamate into glutathione in c-Myc-h-Ras HCCs.**

When we analyzed the glutamine metabolism in *Ldha* KD tumors, we found a significant inhibition of *Gls* expression compared to WT tumors, indicating a lesser glutamine utilization (**Fig. 30**).

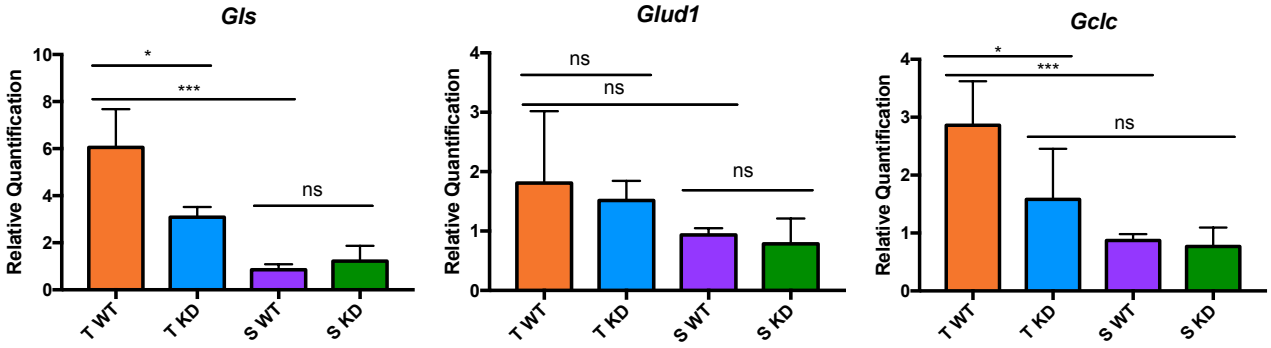


**Fig. 30. qPCR analysis of *Gls, Glud1* and *Gclc* mRNA levels in microdissected tumors (T) and surrounding livers (S) from *Ldha* WT and KD mice. Relative quantification analysis for each gene was calculated by $2^{-\Delta\Delta Ct}$ method. The histogram represents mean values + SD of 5 Tumors and 3 surrounding liver sections. (one way-ANOVA). ns: not significant. **P*<0.05; ****P*<0.001.)**

Next, we investigated the expression of *Glud1* and *Gclc* in the two groups. As reported in **Fig. 30**, *Glud1* expression was not affected in WT or *Ldha* KD tumors. Moreover, no statistically significant differences were detected between tumor and surrounding area, suggesting that the excess of catabolized glutamine is not utilized as a fuel of the TCA cycle.

As regard to *Gclc*, its expression was significantly enhanced in WT tumors compared to the surrounding, while it was down-regulated in KD tumors. These findings suggest that in this hepatocarcinogenesis model the excess of catabolized glutamine in cancer cells is preferentially converted into glutathione in order to protect themselves against oxidative damage and does not fuel the TCA cycle. In addition, they also clearly indicate that this pathway is deeply affected by *Ldha* KD.

To provide further evidence of the impairment of TCA cycle, we checked the expression of malic enzyme, a cytosolic protein that catalyzes the inter-conversion of malate into pyruvate while concomitantly generating NADPH from NADP, and of pyruvate dehydrogenase, responsible for the conversion of pyruvate into acetil-CoA (**Fig. 31A**).

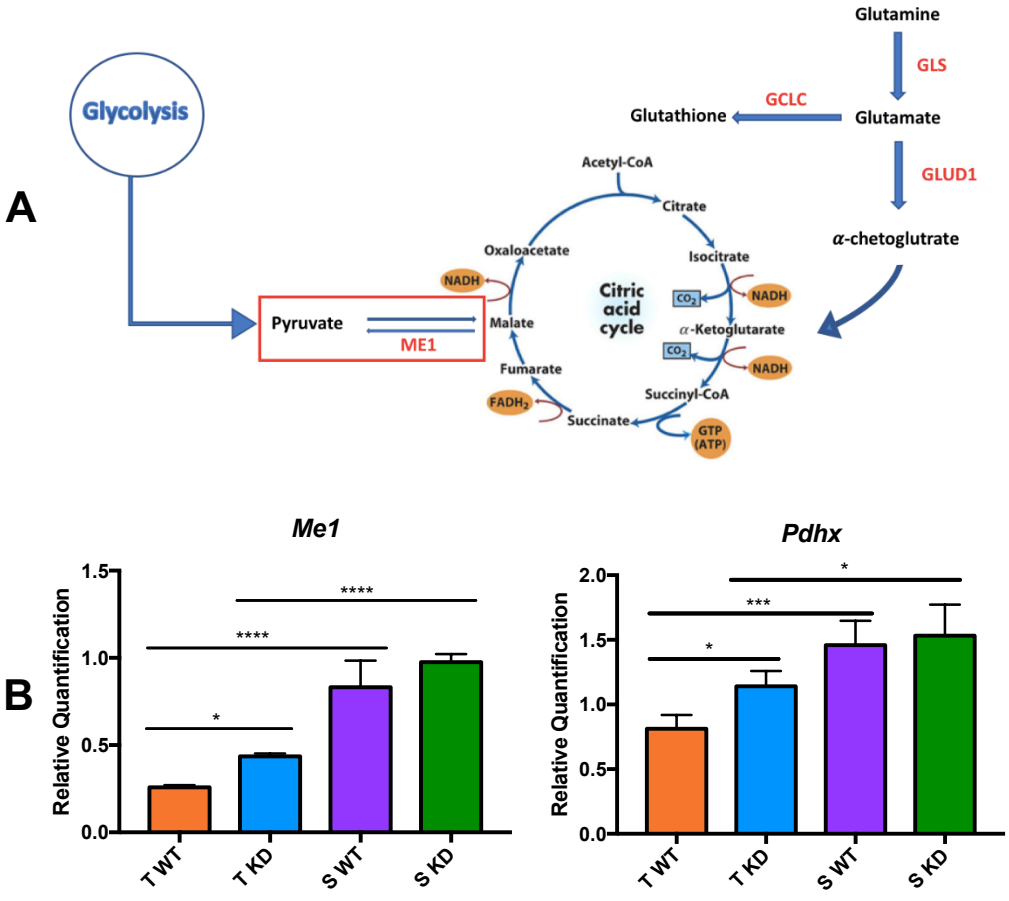


**Fig.31. A) Schematic representation of the dual role of Malic enzyme; B) qPCR analysis of *Me1* mRNA levels of *Me1* and *Pdhx* in laser-microdissected tumors (T) and surrounding livers (S) from *Ldha* WT and KD mice. Relative quantification analysis for each gene was calculated by $2^{-\Delta\Delta Ct}$ method. The histogram represents mean values + SD of 5 Tumors and 3 surrounding liver sections. (one-way ANOVA). **P*<0.05; ****P*<0.001.**

We found that malic enzyme and pyruvate dehydrogenase were downregulated in c-Myc-h-Ras driven tumors compared to peritumoral area. Knock-down of *Ldha* led to a slight increase of *Me-1* and *Pdhx* expression in the tumors compared to WT HCCs. (**Fig. 31B**). The latter results further support the notion of a TCA cycle impairment in HCCs generated by the c-Myc/h-Ras model. Indeed, the conversion of pyruvate into malate – which could enter into TCA cycle - is impaired even in the presence of pyruvate surplus produced by glycolysis. In the same line, the downregulation of pyruvate dehydrogenase prevents the utilization of pyruvate to fuel the TCA cycle.

Finally, to investigate whether up-regulation of the others isoforms of the tetrameric Ldh could compensate for *Ldha* loss, we determined mRNA expression levels of *Ldhb*, *Ldhc* and *Ldhd.* QRT- analysis **(Fig. 32)** showed that *Ldhb* expression was increased in the *Ldha* KD tumors compared to that of WT tumors, However, no significant differences were observed in the expression of *Ldhb* in tumors vs. surrounding peritumoral liver. As to the other two isoforms, the results showed that *Ldhd* expression was lower in both tumor groups compared to the peritumoral tissue, while *Ldhc* was not detected.

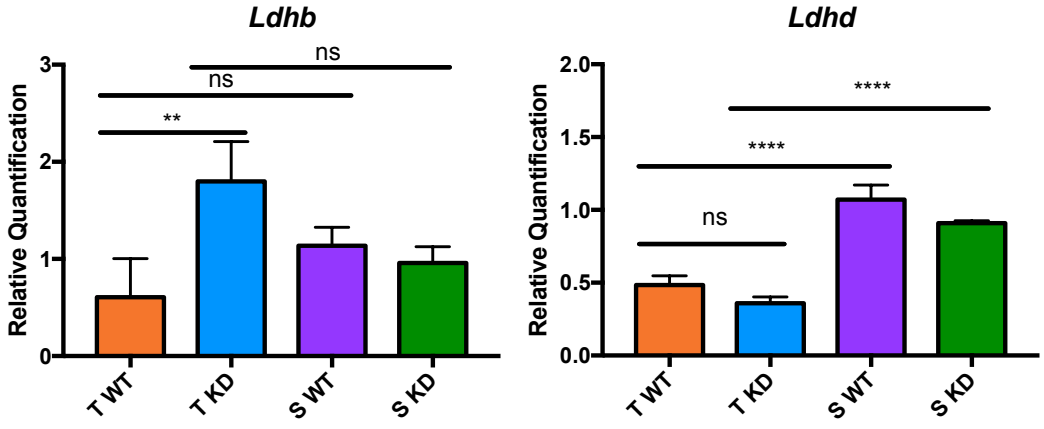


**Fig.32 qPCR analysis of *Ldhb and Ldhd* mRNA levels in laser-microdissected tumors (T) and surrounding livers (S) from *Ldha* WT and *Ldha* KD mice. Relative quantification analysis for each gene was calculated by $2^{-\Delta\Delta Ct}$ method. The histogram represents mean values + SD of 5 Tumors and 3 surrounding liver sections. (one-way ANOVA). **P*<0.05; ****P*<0.001.**

Taken together, these results suggest that the hepatocyte specific *Ldha* knock down in a c-Myc/h-Ras tumor model is able to partially impair the development and progression of hepatic tumors by impairing the metabolic reprogramming towards Warburg phenotype.

## *Ldha* Knockdown and Microenvironment

Since the extrusion of lactate through its transporter Mct4 can influence the extracellular environment, the next step was to investigate if lack of lactate, due to the *Ldha* knock down, could affect cell components of tumor microenvironment (**Fig. 33).**

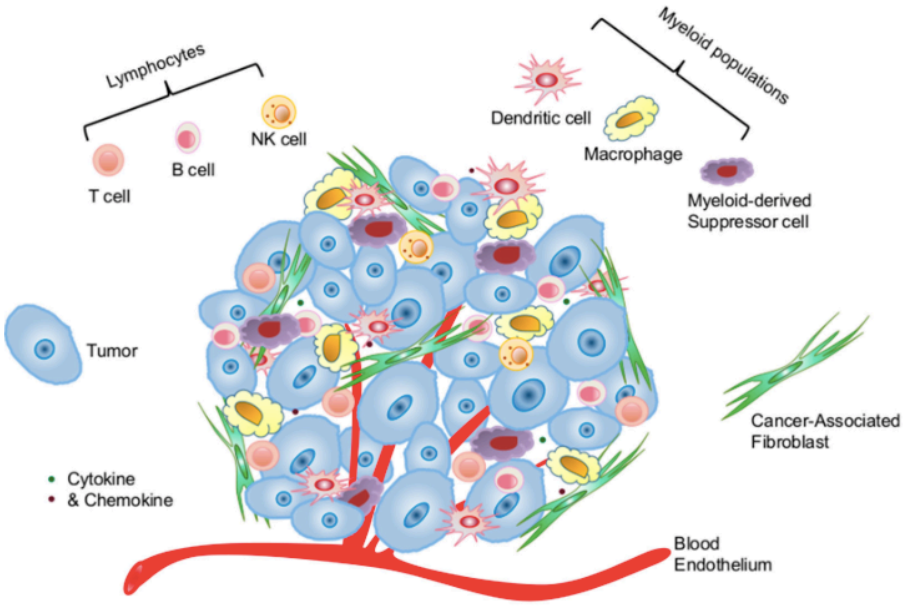


**Figure 33. Schematic representation of tumor microenvironment (95).**

To this aim, FACS analysis was used to study the expression of classical immune cell markers involved in the carcinogenic process.

As shown in **Fig. 34**, *Ldha* KD tumors displayed a decrease in monocyte, granulocytes and neutrophils as shown by the expression of *Ly6g* (Lymphocyte antigen 6 complex locus G6D). On the other hand, *Ldha* KD led to an increase in macrophage population. However, no change of their polarization from M1 to M2 was observed, since the expression of Mhc-II (Class II major histocompatibility complex), a typical M1 marker, and of Cd206 (Cluster of

differentiation 206), whose upregulation is a classical M2 feature, was not modified between the two groups.

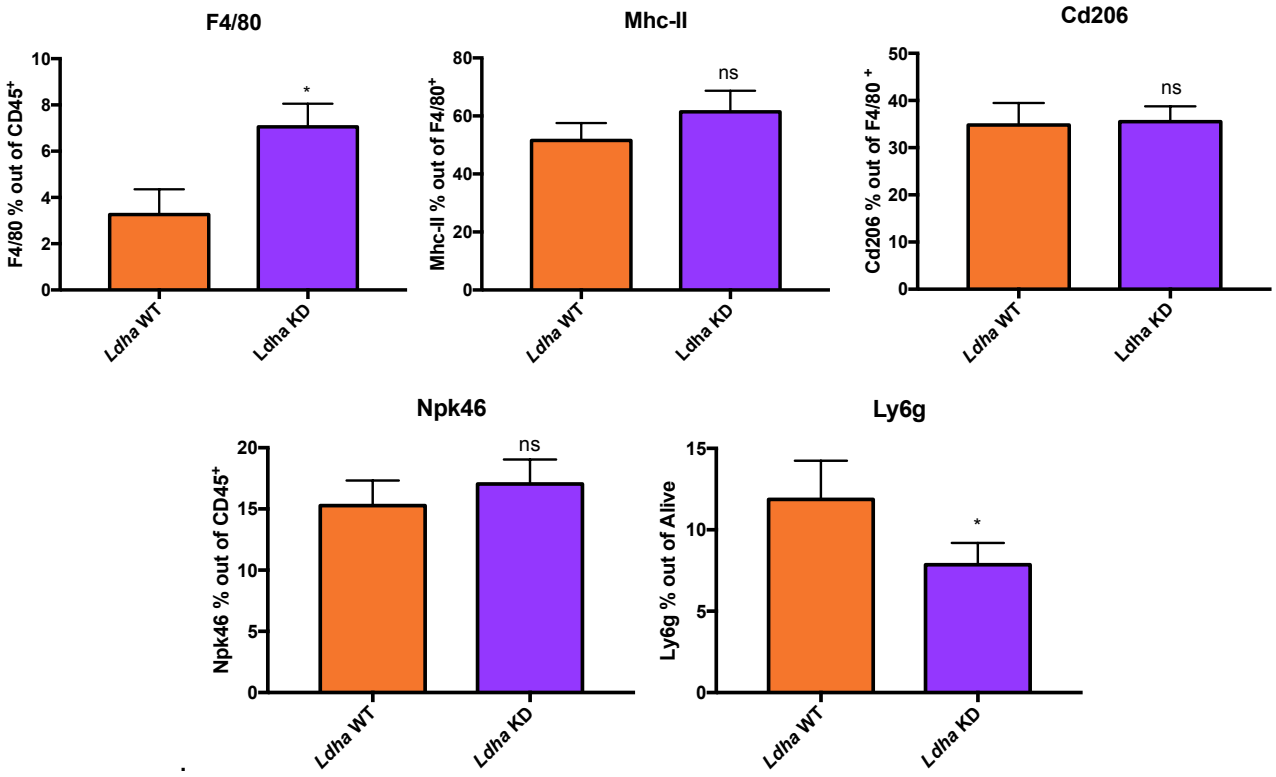


**Figure 34. FACS analysis showing the percentage of F4/80$^+$ macrophage population out of alive cells, Mhc-II$^+$ and Cd206$^+$ population out of F4/80$^+$ cells, Npk46$^+$ population out of Cd45$^+$cells and Ly6g$^+$ population out of alive cells in *Ldha* WT and KD tumors. Ns: not significant; *p < 0.05.**

We also investigated possible changes in lymphocyte cell population. As shown in **Fig. 35**, our results highlighted that lymphocytes were the most affected immune population by *Ldha* knock down in cancer cells. In particular, deprivation of lactate in the extracellular tumor microenvironment caused the loss of Cd8$^+$ with a concomitant increase of Cd4$^+$ lymphocytes (**Fig. 35A**). However, the percentage of Foxp3$^+$/Cd25$^+$ T-reg-activated cells (winged-helix transcription factor forkhead box P3/Cluster of differentiation 25) was not modified (**Fig. 35B**). Loss of Cd8$^+$ lymphocytes in *Ldha* KD mice was further confirmed by immunofluorescence analysis, both in tumoral and peritumoral areas **(Fig. 36),** although Pd1

expression revealed that the exhaustion rate among the two groups remains unaltered **(Fig. 35B).**

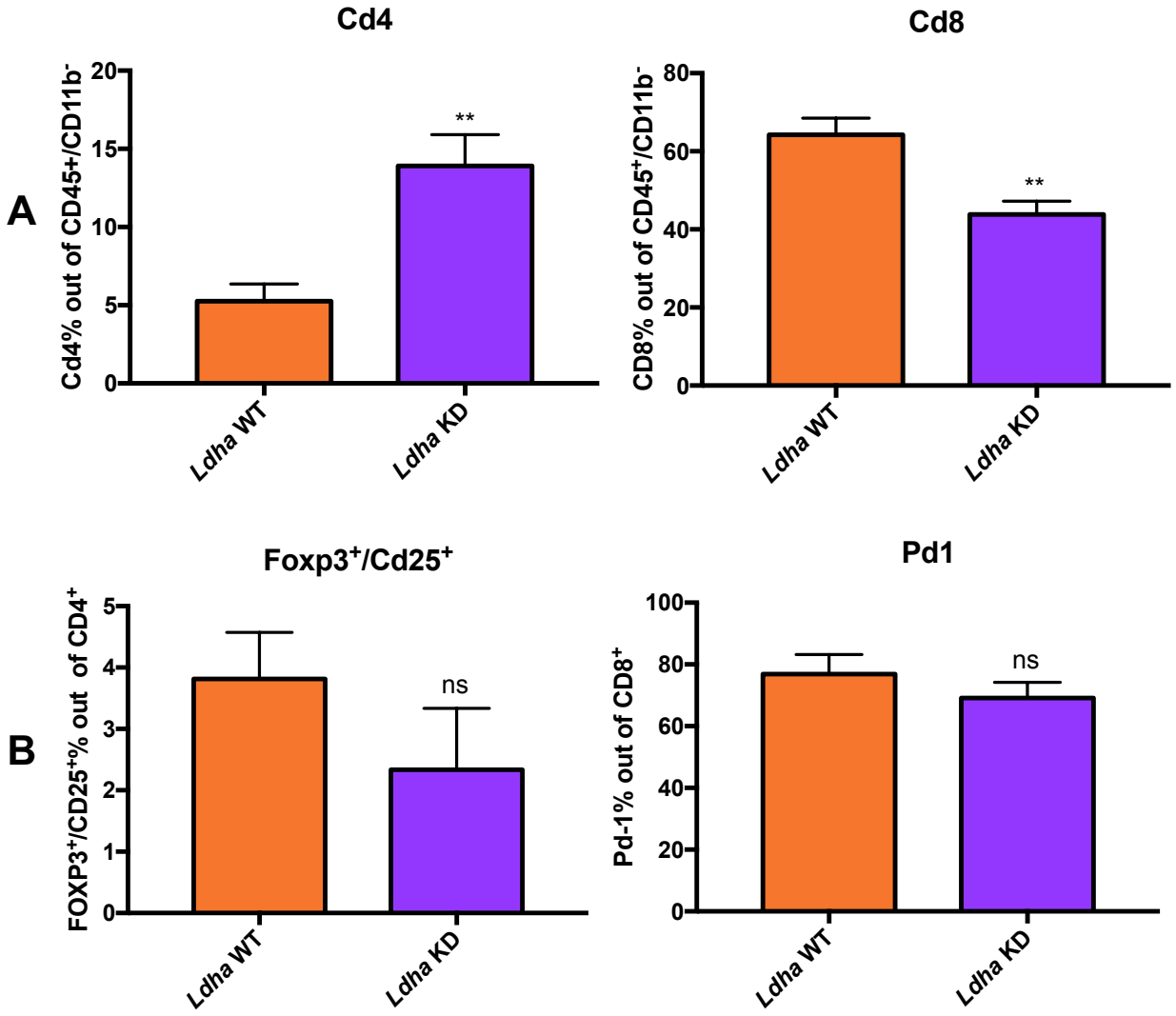


**Figure 35. FACS analysis performed on lymphocytes Cd45$^+$/Cd11b$^-$ cells. A) % of T-helper Cd4$^+$ and cytotoxic Cd8$^+$ cells; B) % of Foxp3$^+$/Cd25$^+$ T-reg population out of Cd4$^+$ cells, and Pd-1$^+$ cells out of Cd8$^+$ population in *Ldha* WT and KD tumors.**

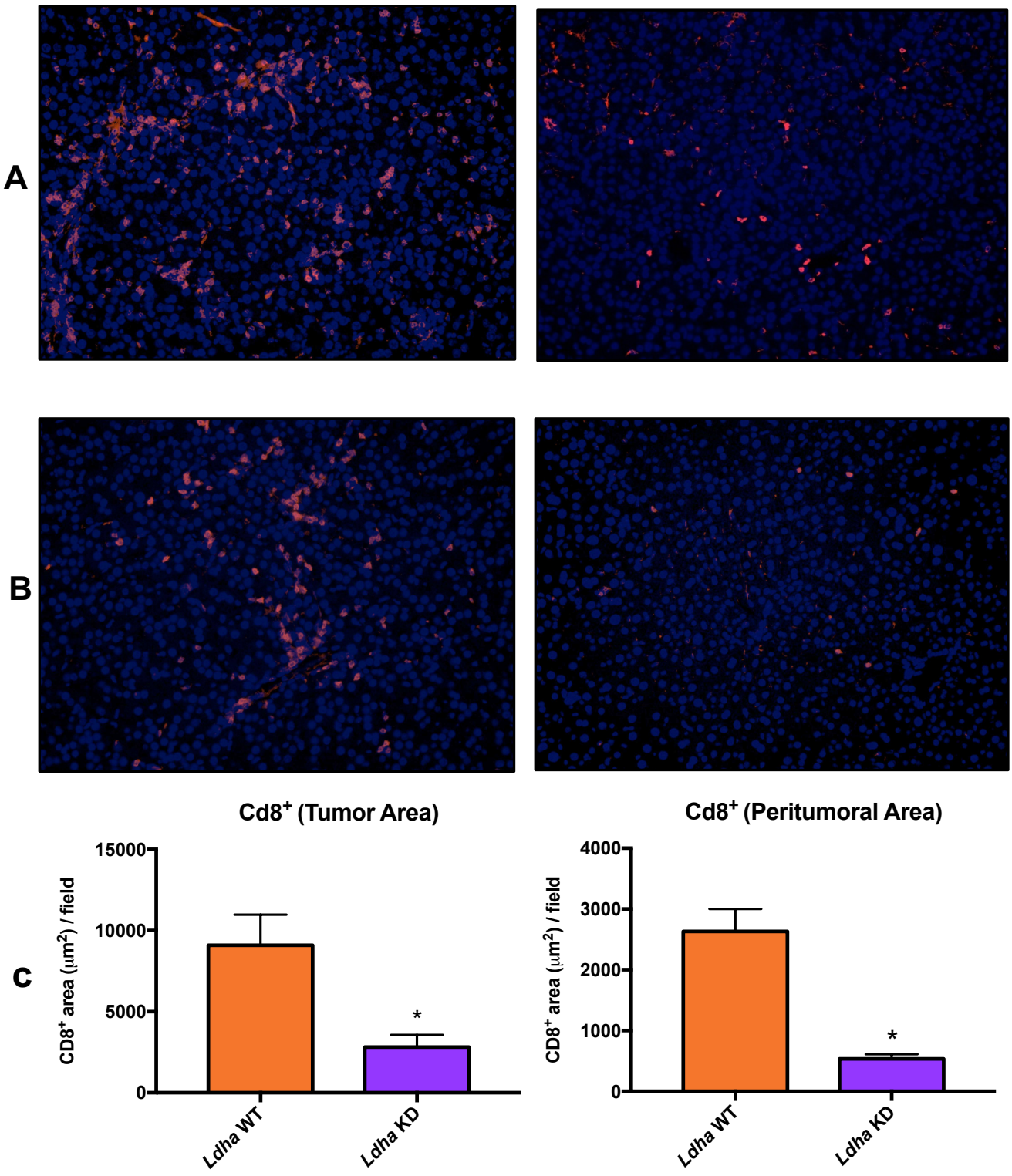


**Figure 36. Immunofluorescence staining showing Cd8⁺ cells in A) *Ldha* WT tumors and, B) *Ldha* KD tumors; Blue (DAPI); Red (Cd8+). C and D: quantification of immunofluorescence results.**

Notably, these findings are in agreement with Ma et al. (96), who demonstrated that the selective loss of Cd4⁺ T lymphocytes promotes cancer development in a nutritional mouse model of hepatocarcinogenesis.

# DISCUSSION

Alterations of different metabolic pathways, such as glycolysis, PPP, glutamine metabolism and mitochondrial respiration have been described in several types of tumor (3). With regard to HCC, it has been reported that more than 600 metabolic genes are consistently altered in human HCCs (23).

Recently, several reports showed that different metabolic alterations may be driven by specific oncogenes. For instance, β-catenin-activated HCCs did not display a Warburg-like phenotype, since they mostly rely on fatty acids oxidation (FAO) and not on glycolysis (97). Conversely, Met-induced liver tumors highlighted an increased glutamine synthesis, while its catabolism was hampered compared to normal livers (72). The overall metabolic reprogramming is still different when looking at HCCs induced by the overexpression of the proto-oncogene c-Myc; indeed, boosted glycolysis, enhanced PPP, and increased glutaminolysis - needed to fuel the TCA cycle no longer supported by glycolytic pyruvate which is preferentially converted into lactate - are the most prominent features of these tumors (75). As a consequence of the increased lactate dehydrogenase A (Ldha) activity, a high content of lactate is produced and extruded form the cell causing the acidification of extracellular microenvironment, a condition thought to promote tumor development and metastasis (14,98–100).

Based on the above observations indicating that metabolic alterations of HCCs appear to be dependent on the nature of the specific oncogene mutation/overexpression - which might explain the extreme heterogeneity of this lethal tumor – the first aim of this study was to investigate the metabolic modifications occurring in HCC generated by a transgenic model consisting of the combination of c-Myc and h-Ras$^{G12V}$, two oncogenes often overexpressed in human HCC (70,71,76,77).

The most significant findings stemming from this work can be summarized as follows:

1) c-Myc/h-Ras driven HCCs underwent an impressive switch towards a glycolytic metabolism and an enhanced PPP; 2) unlike HCCs generated by overexpression of c-Myc alone, glutamine was redirected towards glutathione synthesis instead of TCA cycle, in order to protect cancer cells from oxidative damage. 3) the TCA cycle and OXPHOS were, partially impaired due to the inhibition of succinate dehydrogenase A (Sdha), malic enzyme (Me1) and pyruvate dehydrogenase (Pdhx).

These results obtained in an experimental model whereby the tumors have been generated by two oncogenes commonly overexpressed in human HCC, shed further light on the identification of the exact metabolic alterations occurring in cancer cells taking place during the development of HCC.

The second aim of this thesis was to directly assess the role of Ldha in HCC development, through knockout of *Ldha* gene in the same c-Myc-h-Ras animal model.

We found that the inducible hepatocyte-specific *Ldha* KD led to: 1) an impairment of HCC development as determined by the reduction of both number and size of the tumors, 2) a significant inhibition of the metabolic switch observed in HCCs from Ldha WT animals; 3) downregulation of lactate exporter Mct4, a sign of a diminished release of lactate in the tumoral microenvironment; and, 4) a remarkable increase of $Cd4^+$ lymphocytes which was associated with a reduction of $Cd8^+$ cells.

Overall, the results obtained in this thesis contribute to unveil the potential role of the loss of *Ldha* in impairing HCC development and/or progression. Interestingly, *Ldha* deletion may have profound implications on both the neoplastic cells and the TME. Indeed, as demonstrated by Serganova et al. et al. (101), Ldha promotes stabilization of hypoxia-inducible factor-1a (Hif-1$\alpha$), which, in turn stimulates glycolysis and induces the transcription of vascular endothelial growth factor (Vegf), a fundamental actor in the process of angiogenesis.

Therefore, on the one hand, *Ldha* deletion causes the impairment of the Warburg-like

phenotype, a metabolic condition that represents an advantageous factor for cancer cell growth; at the same time, loss of Ldha activity results in a decreased release of lactate to the extracellular space and a decreased acidification of the TME thus diminishing the invasive capacity of cancer cells and of Vegf. In addition, the finding that Cd4+ lymphocytes were, among different immune cell populations, the most affected cells by deprivation of lactate in the extracellular environment is very interesting as it correlates with tumorigenic process. Indeed, our results are consistent with previous reports by Ma et al. (96) who found that Myc overexpression in mice with non-alcoholic fatty liver induces the selective loss of Cd4+ cells and promotes carcinogenesis, and by Serganova et al. (101) who demonstrated that *Ldha* ablation regulates TME by modulating Hif-1$\alpha$ and promoting the enhancement of CD4+ infiltrate population.

Our data on the impact of *Ldha* on immune response, although preliminary, together with the above mentioned studies (96,101), make possible to imply a critical cross-talk between neoplastic cells and the microenvironment. Indeed, it is possible to speculate that in WT HCC, the release in the microenvironment of both lactate and Vegf promote cancer progression by favouring the process of invasion and neo-angiogenesis, and also immunosuppression in immune competent animals. On the other hand, *Ldha* deletion might deeply affect the tumorigenic process by reducing i) cellular glycolysis and PPP, ii) acidification by reduced lactate extrusion, iii) angiogenesis through down-regulation of Vegf expression, and, iv) also by preserving the anti-neoplastic effect exerted by the CD4+ lymphocytes.

An intriguing finding of our work was that *Ldha* KD tumors, albeit lesser and smaller than WT, still retained a very high proliferative capacity. Although at present we do not have a clear explanation, it is possible that along the time the lack of Ldha can be bypassed by as yet unknown events (i.e. Ldhb up-regulation). If this were to be the case, later time points

than those examined in this thesis would probably show a similar number and burden of tumors between WT and *Ldha* KD mice. To adequately address this hypothesis, further experiments are needed to assess the fate of *Ldha* KD tumors at later time points.

In conclusion, we believe that our results on the effect of *Ldha* loss on cancer development may be potentially useful to design therapeutic strategies based on targeting lactate metabolism in combination with immunotherapy.

Nevertheless, additional studies are mandatory to elucidate the exact molecular mechanisms responsible for the impaired tumor formation caused by *Ldha* KD and its possible impact on TME.

# REFERENCES


1. Hanahan D, Weinberg RA. The hallmarks of cancer. Cell. 2000 Jan;100(1):57–70.
2. Hanahan D, Weinberg RA. Hallmarks of cancer: the next generation. Cell. 2011 Mar;144(5):646–74.
3. Pavlova NN, Thompson CB. The Emerging Hallmarks of Cancer Metabolism. Cell Metab. 2016 Jan;23(1):27–47.
4. Vander Heiden MG, Cantley LC, Thompson CB. Understanding the Warburg effect: the metabolic requirements of cell proliferation. Science. 2009 May;324(5930):1029–33.
5. Warburg O, Wind F, Negelein E. THE METABOLISM OF TUMORS IN THE BODY. J Gen Physiol. 1927 Mar;8(6):519–30.
6. WARBURG O. On the origin of cancer cells. Science. 1956 Feb;123(3191):309–14.
7. WARBURG O. On respiratory impairment in cancer cells. Science. 1956 Aug;124(3215):269–70.
8. Weinhouse S. The Warburg hypothesis fifty years later. Zeitschrift fur Krebsforsch und Klin Onkol Cancer Res Clin Oncol. 1976;87(2):115–26.
9. Moreno-Sánchez R, Rodríguez-Enríquez S, Marín-Hernández A, Saavedra E. Energy metabolism in tumor cells. FEBS J. 2007 Mar;274(6):1393–418.
10. DeBerardinis RJ, Lum JJ, Hatzivassiliou G, Thompson CB. The biology of cancer: metabolic reprogramming fuels cell growth and proliferation. Cell Metab. 2008 Jan;7(1):11–20.
11. Gatenby RA, Gillies RJ. Why do cancers have high aerobic glycolysis? Nat Rev Cancer. 2004 Nov;4(11):891–9.
12. Mishra D, Banerjee D. Lactate Dehydrogenases as Metabolic Links between Tumor and Stroma in the Tumor Microenvironment. Cancers (Basel). 2019 May;11(6).
13. de la Cruz-López KG, Castro-Muñoz LJ, Reyes-Hernández DO, García-Carrancá A, Manzo-Merino J. Lactate in the Regulation of Tumor Microenvironment and Therapeutic Approaches. Front Oncol. 2019;9:1143.
14. Consoli A, Nurjhan N, Reilly JJJ, Bier DM, Gerich JE. Contribution of liver and skeletal muscle to alanine and lactate metabolism in humans. Am J Physiol. 1990 Nov;259(5 Pt 1):E677-84.
15. Goetzman ES, Prochownik E V. The Role for Myc in Coordinating Glycolysis, Oxidative Phosphorylation, Glutaminolysis, and Fatty Acid Metabolism in Normal and Neoplastic Tissues. Front Endocrinol (Lausanne). 2018;9:129.
16. Hsu PP, Sabatini DM. Cancer cell metabolism: Warburg and beyond. Cell. 2008 Sep;134(5):703–7.
17. Dang C V, Semenza GL. Oncogenic alterations of metabolism. Trends Biochem Sci. 1999 Feb;24(2):68–72.
18. Ramanathan A, Wang C, Schreiber SL. Perturbational profiling of a cell-line model of tumorigenesis by using metabolic measurements. Proc Natl Acad Sci U S A. 2005 Apr;102(17):5992–7.
19. Yun J, Rago C, Cheong I, Pagliarini R, Angenendt P, Rajagopalan H, et al. Glucose

deprivation contributes to the development of KRAS pathway mutations in tumor cells. Science. 2009 Sep;325(5947):1555–9.

20. Manning BD, Cantley LC. AKT/PKB signaling: navigating downstream. Cell. 2007 Jun;129(7):1261–74.
21. Gordan JD, Thompson CB, Simon MC. HIF and c-Myc: sibling rivals for control of cancer cell metabolism and proliferation. Cancer Cell. 2007 Aug;12(2):108–13.
22. Son J, Lyssiotis CA, Ying H, Wang X, Hua S, Ligorio M, et al. Glutamine supports pancreatic cancer growth through a KRAS-regulated metabolic pathway. Nature. 2013 Apr;496(7443):101–5.
23. Nwosu ZC, Megger DA, Hammad S, Sitek B, Roessler S, Ebert MP, et al. Identification of the Consistently Altered Metabolic Targets in Human Hepatocellular Carcinoma. Cell Mol Gastroenterol Hepatol. 2017 Sep;4(2):303-323.e1.
24. Liu T, Yin H. PDK1 promotes tumor cell proliferation and migration by enhancing the Warburg effect in non-small cell lung cancer. Oncol Rep. 2017 Jan;37(1):193–200.
25. Forner A, Llovet JM, Bruix J. Hepatocellular carcinoma. Lancet (London, England). 2012 Mar;379(9822):1245–55.
26. Bray F, Ferlay J, Soerjomataram I, Siegel RL, Torre LA, Jemal A. Global cancer statistics 2018: GLOBOCAN estimates of incidence and mortality worldwide for 36 cancers in 185 countries. CA Cancer J Clin. 2018 Nov;68(6):394–424.
27. Llovet JM, Ricci S, Mazzaferro V, Hilgard P, Gane E, Blanc J-F, et al. Sorafenib in advanced hepatocellular carcinoma. N Engl J Med. 2008 Jul;359(4):378–90.
28. El-Serag HB, Rudolph KL. Hepatocellular carcinoma: epidemiology and molecular carcinogenesis. Gastroenterology. 2007 Jun;132(7):2557–76.
29. Llovet JM, Zucman-Rossi J, Pikarsky E, Sangro B, Schwartz M, Sherman M, et al. Hepatocellular carcinoma. Nat Rev Dis Prim. 2016 Apr;2:16018.
30. McGlynn KA, Petrick JL, London WT. Global epidemiology of hepatocellular carcinoma: an emphasis on demographic and regional variability. Clin Liver Dis. 2015 May;19(2):223–38.
31. Macek Jilkova Z, Kurma K, Decaens T. Animal Models of Hepatocellular Carcinoma: The Role of Immune System and Tumor Microenvironment. Cancers (Basel). 2019 Oct;11(10).
32. Kiyosawa K, Sodeyama T, Tanaka E, Gibo Y, Yoshizawa K, Nakano Y, et al. Interrelationship of blood transfusion, non-A, non-B hepatitis and hepatocellular carcinoma: analysis by detection of antibody to hepatitis C virus. Hepatology. 1990 Oct;12(4 Pt 1):671–5.
33. McMahon BJ. Epidemiology and natural history of hepatitis B. Semin Liver Dis. 2005;25 Suppl 1:3–8.
34. Pons-Renedo F, Llovet JM. Hepatocellular carcinoma: a clinical update. MedGenMed. 2003 Jul;5(3):11.
35. Bruix J, Sherman M. Management of hepatocellular carcinoma. Hepatology. 2005 Nov;42(5):1208–36.
36. Bruix J, Qin S, Merle P, Granito A, Huang Y-H, Bodoky G, et al. Regorafenib for patients with hepatocellular carcinoma who progressed on sorafenib treatment (RESORCE): a randomised, double-blind, placebo-controlled, phase 3 trial. Lancet (London, England). 2017 Jan;389(10064):56–66.

37. Finn RS, Merle P, Granito A, Huang Y-H, Bodoky G, Pracht M, et al. Outcomes of sequential treatment with sorafenib followed by regorafenib for HCC: Additional analyses from the phase III RESORCE trial. J Hepatol. 2018 Aug;69(2):353–8.

38. Nwosu ZC, Battello N, Rothley M, Piorońska W, Sitek B, Ebert MP, et al. Liver cancer cell lines distinctly mimic the metabolic gene expression pattern of the corresponding human tumours. J Exp Clin Cancer Res. 2018 Sep;37(1):211.

39. Serra M, Columbano A, Perra A, Kowalik MA. Animal Models: A Useful Tool to Unveil Metabolic Changes in Hepatocellular Carcinoma. Cancers (Basel) [Internet]. 2020 Nov 10 [cited 2020 Nov 19];12(11):3318. Available from: https://www.mdpi.com/2072-6694/12/11/3318

40. De Minicis S, Kisseleva T, Francis H, Baroni GS, Benedetti A, Brenner D, et al. Liver carcinogenesis: rodent models of hepatocarcinoma and cholangiocarcinoma. Dig liver Dis Off J Ital Soc Gastroenterol Ital Assoc Study Liver. 2013 Jun;45(6):450–9.

41. Cho K, Ro SW, Seo SH, Jeon Y, Moon H, Kim DY, et al. Genetically Engineered Mouse Models for Liver Cancer. Cancers (Basel). 2019 Dec;12(1).

42. Gopinathan A, Tuveson DA. The use of GEM models for experimental cancer therapeutics. Vol. 1, Disease models & mechanisms. 2008. p. 83–6.

43. Kim H, Kim M, Im S-K, Fang S. Mouse Cre-LoxP system: general principles to determine tissue-specific roles of target genes. Lab Anim Res. 2018 Dec;34(4):147–59.

44. Hardouin SN, Nagy A. Mouse models for human disease. Clin Genet. 2000 Apr;57(4):237–44.

45. Chen X, Calvisi DF. Hydrodynamic Transfection for Generation of Novel Mouse Models for Liver Cancer Research. Am J Pathol [Internet]. 2014;184(4):912–23. Available from: http://www.sciencedirect.com/science/article/pii/S0002944014000078

46. Liu F, Song Y, Liu D. Hydrodynamics-based transfection in animals by systemic administration of plasmid DNA. Gene Ther. 1999 Jul;6(7):1258–66.

47. Perkins EJ, Bao W, Guan X, Ang C-Y, Wolfinger RD, Chu T-M, et al. Comparison of transcriptional responses in liver tissue and primary hepatocyte cell cultures after exposure to hexahydro-1, 3, 5-trinitro-1, 3, 5-triazine. BMC Bioinformatics. 2006 Dec;7 Suppl 4(Suppl 4):S22.

48. Uhlen M, Zhang C, Lee S, Sjöstedt E, Fagerberg L, Bidkhori G, et al. A pathology atlas of the human cancer transcriptome. Science. 2017 Aug;357(6352).

49. Peng X, Chen Z, Farshidfar F, Xu X, Lorenzi PL, Wang Y, et al. Molecular Characterization and Clinical Relevance of Metabolic Expression Subtypes in Human Cancers. Cell Rep. 2018 Apr;23(1):255-269.e4.

50. Hu J, Locasale JW, Bielas JH, O'Sullivan J, Sheahan K, Cantley LC, et al. Heterogeneity of tumor-induced gene expression changes in the human metabolic network. Nat Biotechnol. 2013 Jun;31(6):522–9.

51. DeBerardinis RJ, Chandel NS. Fundamentals of cancer metabolism. Sci Adv [Internet]. 2016 May 1;2(5):e1600200. Available from: http://advances.sciencemag.org/content/2/5/e1600200.abstract

52. Björnson E, Mukhopadhyay B, Asplund A, Pristovsek N, Cinar R, Romeo S, et al. Stratification of Hepatocellular Carcinoma Patients Based on Acetate Utilization. Cell Rep [Internet]. 2015;13(9):2014–26. Available from:

http://www.sciencedirect.com/science/article/pii/S2211124715012152

53. Amann T, Maegdefrau U, Hartmann A, Agaimy A, Marienhagen J, Weiss TS, et al. GLUT1 expression is increased in hepatocellular carcinoma and promotes tumorigenesis. Am J Pathol. 2009 Apr;174(4):1544–52.

54. Amann T, Hellerbrand C. GLUT1 as a therapeutic target in hepatocellular carcinoma. Expert Opin Ther Targets. 2009 Dec;13(12):1411–27.

55. Chen H-L, OuYang H-Y, Le Y, Jiang P, Tang H, Yu Z-S, et al. Aberrant MCT4 and GLUT1 expression is correlated with early recurrence and poor prognosis of hepatocellular carcinoma after hepatectomy. Cancer Med. 2018 Nov;7(11):5339–50.

56. Kowalik MA, Guzzo G, Morandi A, Perra A, Menegon S, Masgras I, et al. Metabolic reprogramming identifies the most aggressive lesions at early phases of hepatic carcinogenesis. Oncotarget. 2016 May;7(22):32375–93.

57. Fang Z, He L, Jia H, Huang Q, Chen D, Zhang Z. The miR-383-LDHA axis regulates cell proliferation, invasion and glycolysis in hepatocellular cancer. Iran J Basic Med Sci. 2017 Feb;20(2):187–92.

58. Sheng SL, Liu JJ, Dai YH, Sun XG, Xiong XP, Huang G. Knockdown of lactate dehydrogenase A suppresses tumor growth and metastasis of human hepatocellular carcinoma. FEBS J. 2012 Oct;279(20):3898–910.

59. Gao H-J, Zhao M-C, Zhang Y-J, Zhou D-S, Xu L, Li G-B, et al. Monocarboxylate transporter 4 predicts poor prognosis in hepatocellular carcinoma and is associated with cell proliferation and migration. J Cancer Res Clin Oncol. 2015 Jul;141(7):1151–62.

60. De Matteis S, Ragusa A, Marisi G, De Domenico S, Casadei Gardini A, Bonafè M, et al. Aberrant Metabolism in Hepatocellular Carcinoma Provides Diagnostic and Therapeutic Opportunities. Egea J, editor. Oxid Med Cell Longev [Internet]. 2018;2018:7512159. Available from: https://doi.org/10.1155/2018/7512159

61. Bard-Chapeau EA, Nguyen A-T, Rust AG, Sayadi A, Lee P, Chua BQ, et al. Transposon mutagenesis identifies genes driving hepatocellular carcinoma in a chronic hepatitis B mouse model. Nat Genet. 2014 Jan;46(1):24–32.

62. Meyer N, Penn LZ. Reflecting on 25 years with MYC. Nat Rev Cancer. 2008 Dec;8(12):976–90.

63. Thompson NL, Mead JE, Braun L, Goyette M, Shank PR, Fausto N. Sequential protooncogene expression during rat liver regeneration. Cancer Res. 1986 Jun;46(6):3111–7.

64. Fausto N, Mead JE, Braun L, Thompson NL, Panzica M, Goyette M, et al. Proto-oncogene expression and growth factors during liver regeneration. Symp Fundam Cancer Res. 1986;39:69–86.

65. Makino R, Hayashi K, Sugimura T. C-myc transcript is induced in rat liver at a very early stage of regeneration or by cycloheximide treatment. Nature. 1984 Aug;310(5979):697–8.

66. Shachaf CM, Kopelman AM, Arvanitis C, Karlsson A, Beer S, Mandl S, et al. MYC inactivation uncovers pluripotent differentiation and tumour dormancy in hepatocellular cancer. Nature. 2004 Oct;431(7012):1112–7.

67. Calvisi DF, Thorgeirsson SS. Molecular mechanisms of hepatocarcinogenesis in transgenic mouse models of liver cancer. Toxicol Pathol. 2005;33(1):181–4.

68. Kaposi-Novak P, Libbrecht L, Woo HG, Lee Y-H, Sears NC, Coulouarn C, et al. Central role of c-Myc during malignant conversion in human hepatocarcinogenesis. Cancer Res. 2009 Apr;69(7):2775–82.

69. Lim L, Balakrishnan A, Huskey N, Jones KD, Jodari M, Ng R, et al. MicroRNA-494 within an oncogenic microRNA megacluster regulates G1/S transition in liver tumorigenesis through suppression of mutated in colorectal cancer. Hepatology. 2014 Jan;59(1):202–15.

70. Kawate S, Fukusato T, Ohwada S, Watanuki A, Morishita Y. Amplification of c-myc in hepatocellular carcinoma: correlation with clinicopathologic features, proliferative activity and p53 overexpression. Oncology. 1999;57(2):157–63.

71. Schlaeger C, Longerich T, Schiller C, Bewerunge P, Mehrabi A, Toedt G, et al. Etiology-dependent molecular mechanisms in human hepatocarcinogenesis. Hepatology. 2008 Feb;47(2):511–20.

72. Yuneva MO, Fan TWM, Allen TD, Higashi RM, Ferraris D V, Tsukamoto T, et al. The metabolic profile of tumors depends on both the responsible genetic lesion and tissue type. Cell Metab. 2012 Feb;15(2):157–70.

73. Osthus RC, Shim H, Kim S, Li Q, Reddy R, Mukherjee M, et al. Deregulation of glucose transporter 1 and glycolytic gene expression by c-Myc. J Biol Chem. 2000 Jul;275(29):21797–800.

74. Le A, Lane AN, Hamaker M, Bose S, Gouw A, Barbi J, et al. Glucose-independent glutamine metabolism via TCA cycling for proliferation and survival in B cells. Cell Metab. 2012 Jan;15(1):110–21.

75. Anderton B, Camarda R, Balakrishnan S, Balakrishnan A, Kohnz RA, Lim L, et al. MYC-driven inhibition of the glutamate-cysteine ligase promotes glutathione depletion in liver cancer. EMBO Rep. 2017 Apr;18(4):569–85.

76. Newell P, Toffanin S, Villanueva A, Chiang DY, Minguez B, Cabellos L, et al. Ras pathway activation in hepatocellular carcinoma and anti-tumoral effect of combined sorafenib and rapamycin in vivo. J Hepatol [Internet]. 2009;51(4):725–33. Available from: http://www.sciencedirect.com/science/article/pii/S0168827809003213

77. Calvisi DF, Ladu S, Gorden A, Farina M, Conner EA, Lee J, et al. Ubiquitous Activation of Ras and Jak/Stat Pathways in Human HCC. Gastroenterology [Internet]. 2006;130(4):1117–28. Available from: http://www.sciencedirect.com/science/article/pii/S0016508506000072

78. Jonkers J, Berns A. Conditional mouse models of sporadic cancer. Nat Rev Cancer. 2002 Apr;2(4):251–65.

79. Tipanee J, Di Matteo M, Tulalamba W, Samara-Kuko E, Keirsse J, Van Ginderachter JA, et al. Validation of miR-20a as a Tumor Suppressor Gene in Liver Carcinoma Using Hepatocyte-Specific Hyperactive piggyBac Transposons. Mol Ther Nucleic Acids. 2020 Mar;19:1309–29.

80. King KL, Hwang JJ, Chau GY, Tsay SH, Chi CW, Lee TG, et al. Ki-67 expression as a prognostic marker in patients with hepatocellular carcinoma. J Gastroenterol Hepatol. 1998 Mar;13(3):273–9.

81. Mitsuishi Y, Taguchi K, Kawatani Y, Shibata T, Nukiwa T, Aburatani H, et al. Nrf2 redirects glucose and glutamine into anabolic pathways in metabolic reprogramming. Cancer Cell. 2012 Jul;22(1):66–79.

82. de La Coste A, Romagnolo B, Billuart P, Renard CA, Buendia MA, Soubrane O, et

al. Somatic mutations of the beta-catenin gene are frequent in mouse and human hepatocellular carcinomas. Proc Natl Acad Sci U S A. 1998 Jul;95(15):8847–51.

83. Devereux TR, Stern MC, Flake GP, Yu MC, Zhang ZQ, London SJ, et al. CTNNB1 mutations and beta-catenin protein accumulation in human hepatocellular carcinomas associated with high exposure to aflatoxin B1. Mol Carcinog. 2001 Jun;31(2):68–73.

84. Zucman-Rossi J, Benhamouche S, Godard C, Boyault S, Grimber G, Balabaud C, et al. Differential effects of inactivated Axin1 and activated beta-catenin mutations in human hepatocellular carcinomas. Oncogene. 2007 Feb;26(5):774–80.

85. Lee Y-K, Lim JJ, Jeoun U-W, Min S, Lee E-B, Kwon SM, et al. Lactate-mediated mitoribosomal defects impair mitochondrial oxidative phosphorylation and promote hepatoma cell invasiveness. J Biol Chem. 2017 Dec;292(49):20208–17.

86. Graves JA, Wang Y, Sims-Lucas S, Cherok E, Rothermund K, Branca MF, et al. Mitochondrial structure, function and dynamics are temporally controlled by c-Myc. PLoS One. 2012;7(5):e37699.

87. Li F, Wang Y, Zeller KI, Potter JJ, Wonsey DR, O'Donnell KA, et al. Myc stimulates nuclearly encoded mitochondrial genes and mitochondrial biogenesis. Mol Cell Biol. 2005 Jul;25(14):6225–34.

88. Wang H, Lu J, Dolezal J, Kulkarni S, Zhang W, Chen A, et al. Inhibition of hepatocellular carcinoma by metabolic normalization. PLoS One. 2019;14(6):e0218186.

89. Iverson TM. Catalytic mechanisms of complex II enzymes: A structural perspective. Biochim Biophys Acta - Bioenerg [Internet]. 2013;1827(5):648–57. Available from: http://www.sciencedirect.com/science/article/pii/S0005272812010316

90. Cecchini G. Function and structure of complex II of the respiratory chain. Annu Rev Biochem. 2003;72:77–109.

91. Itoh K, Wakabayashi N, Katoh Y, Ishii T, Igarashi K, Engel JD, et al. Keap1 represses nuclear activation of antioxidant responsive elements by Nrf2 through binding to the amino-terminal Neh2 domain. Genes Dev. 1999 Jan;13(1):76–86.

92. Moi P, Chan K, Asunis I, Cao A, Kan YW. Isolation of NF-E2-related factor 2 (Nrf2), a NF-E2-like basic leucine zipper transcriptional activator that binds to the tandem NF-E2/AP1 repeat of the beta-globin locus control region. Proc Natl Acad Sci U S A. 1994 Oct;91(21):9926–30.

93. Schwickert G, Walenta S, Sundfør K, Rofstad EK, Mueller-Klieser W. Correlation of high lactate levels in human cervical cancer with incidence of metastasis. Cancer Res. 1995 Nov;55(21):4757–9.

94. Walenta S, Salameh A, Lyng H, Evensen JF, Mitze M, Rofstad EK, et al. Correlation of high lactate levels in head and neck tumors with incidence of metastasis. Am J Pathol. 1997 Feb;150(2):409–15.

95. Cui Y, Guo G. Immunomodulatory Function of the Tumor Suppressor p53 in Host Immune Response and the Tumor Microenvironment. Int J Mol Sci. 2016 Nov;17(11).

96. Ma C, Kesarwala AH, Eggert T, Medina-Echeverz J, Kleiner DE, Jin P, et al. NAFLD causes selective CD4(+) T lymphocyte loss and promotes hepatocarcinogenesis. Nature. 2016 Mar;531(7593):253–7.

97. Senni N, Savall M, Cabrerizo Granados D, Alves-Guerra M-C, Sartor C, Lagoutte I,

et al. β-catenin-activated hepatocellular carcinomas are addicted to fatty acids. Gut. 2019 Feb;68(2):322–34.

98. Le A, Cooper CR, Gouw AM, Dinavahi R, Maitra A, Deck LM, et al. Inhibition of lactate dehydrogenase A induces oxidative stress and inhibits tumor progression. Proc Natl Acad Sci U S A. 2010 Feb;107(5):2037–42.

99. Fantin VR, St-Pierre J, Leder P. Attenuation of LDH-A expression uncovers a link between glycolysis, mitochondrial physiology, and tumor maintenance. Cancer Cell. 2006 Jun;9(6):425–34.

100. Rizwan A, Serganova I, Khanin R, Karabeber H, Ni X, Thakur S, et al. Relationships between LDH-A, lactate, and metastases in 4T1 breast tumors. Clin cancer Res an Off J Am Assoc Cancer Res. 2013 Sep;19(18):5158–69.

101. Serganova I, Cohen IJ, Vemuri K, Shindo M, Maeda M, Mane M, et al. LDH-A regulates the tumor microenvironment via HIF-signaling and modulates the immune response. PLoS One. 2018;13(9):e0203965.